Anisotropy and Modal Hybridization in Infrared Nanophotonics using Low-Symmetry Materials

Mingze He,[1] Thomas G. Folland,[2] Jiahua Duan,[3,4] Pablo Alonso-González,[3,4] Simone De Liberato,[5] Alexander Paarmann,[6] Joshua D. Caldwell[1,7*]

1. Department of Mechanical Engineering, Vanderbilt University, 101 Olin Hall, 2400 Highland Ave, Nashville, TN 37205, USA
2. Department of Physics and Astronomy, The University of Iowa, Iowa City, Iowa, 52241, USA
3. Department of Physics, University of Oviedo, Oviedo 33006, Spain.
4. Center of Research on Nanomaterials and Nanotechnology, CINN (CSIC-Universidad de Oviedo), El Entrego 33940, Spain.
5. School of Physics and Astronomy, University of Southampton, Southampton, SO17 1BJ, United Kingdom
6. Department of Physical Chemistry, Fritz Haber Institute of the Max Planck Society, Berlin, 14195, Germany
7. Interdisciplinary Materials Science Program, Vanderbilt University, 101 Olin Hall, 2400 Highland Ave, Nashville, TN 37205, USA

Corresponding author: Joshua D. Caldwell, josh.caldwell@vanderbilt.edu

Abstract:

Anisotropy has been a key property employed in the design of optical components for hundreds of years. However, in recent years there has been growing interest into polaritons supported within anisotropic (low crystal symmetry) materials for their ability to compress light to smaller, deeply sub-wavelength dimensions. While historically the first anisotropic polaritons probed were hyperbolic modes, research into anisotropic materials has recently turned towards hybrid materials and optical modes, employing phenomena such as phonon confinement, polaritonic strong coupling, and Moiré structures to design the optical properties. In this Perspective, we will briefly introduce the physics and theories of polariton anisotropy, review recently investigated anisotropic and two-dimensional materials, and then move on to a discussion of approaches towards realizing hybrid modes and identifying new materials. Based on the results from the past few years, we extend these discussions to highlight outstanding challenges and outline what we perceive as promising paths to further explore the potential for polariton anisotropy and hybrid systems in future nanophotonic optical devices.

Keywords:

Polaritons, anisotropy, hyperbolic

Introduction

Anisotropy is at the heart of a broad range of optical phenomena, most notably using polarization manipulation in waveplates and in magneto-optic effects such as Kerr and Faraday rotation. Optical anisotropy means that light polarized along different crystal axes propagates within the medium at different velocities and thus, wavelengths, due to the variation in the dielectric permittivity tensors. As such, this gives rise to a so-called 'fast' and 'slow' axis for light propagation in the medium, with the differences between the tensor magnitudes (real part of the permittivity at a given frequency) driving the degree of polarization rotation as a function of pathlength (*e.g.*, waveplate thickness). Historically, anisotropic dielectric species such as calcite have been employed for broadband applications as the dielectric function is also nominally constant over a broad spectral range. In such materials the degree of anisotropy (defined as the difference in refractive index along the directions, Δn) is typically small, only on the order of 0.1. Yet, near a strong material resonance (*e.g.,* a crystal vibration), giant birefringence can be observed,[1] illustrating dramatic differences in the refractive index along orthogonal directions $\Delta n > 1$, enhancing material anisotropy. In extreme cases, such resonances can induce the permittivity tensor to become negative over specific spectral ranges, resulting in metallic behavior and the strong reflection of light. Further, such a negative permittivity is necessary for the opportunity to stimulate and exploit surface polaritons, *i.e.*, quasi-particles comprised of strongly coupled coherently oscillating charges in matter with a photon. In the infrared (IR), coupling light with coherent free-carrier oscillations (*e.g.*, conduction electrons or holes) gives rise to surface plasmon polaritons (SPPs), while polar optic phonons offer the opportunity to stimulate surface phonon polaritons (SPhPs).[2–5] These surface waves are exemplified by a polariton wavelength (λ_P), which is shorter than light of the same frequency in free space (λ_{FS}), thereby serving as the basis for IR nanophotonics and for deeply sub-diffractional and compact optical components. Beyond the intriguing physics within such simple polaritonic materials, these surface waves are significantly modified within strongly anisotropic materials that supporting them, giving rise to exciting phenomena such as hyperbolicity[6] (discussed below), which enables new paradigms in optical engineering unattainable with traditional refractive optics.

In certain extremely anisotropic materials (lower symmetry), resonances can cause the dielectric permittivity to be negative along certain crystal axes, while remaining positive along others. Under such conditions the material simultaneously behaves as an optical metal (negative real part of the permittivity tensor, $Re(\varepsilon) < 0$) and a dielectric ($Re(\varepsilon) > 0$), a phenomenon known as hyperbolicity.[6,7] This form of

anisotropy has seen intense interest in recent years following the first observation of naturally hyperbolic materials,[8–12] as it offers significantly improved compression of light and does so within the volume, rather than surface of the medium, as well as enabling the manipulation of properties not inherent to isotropic materials. Notably, the role that strong material anisotropy plays in controlling polariton propagation has led to exciting new developments such as in-plane hyperbolicity,[13–16] and so-called 'ghost'[17] and 'shear'[18] polaritons in low symmetry off-cut crystals and monoclinic and triclinic crystals, respectively. However, in addition to hyperbolic behavior, advances in artificial stacking and structuring of materials (both isotropic and anisotropic in nature) through heterostructure and superlattice fabrication have given rise to hybrid materials such as the electromagnetic[19–21] or crystalline hybrid materials,[20–23] as well as the field of twist-optics.[24,25] Such discoveries have enabled advances in our understanding of light-matter interactions at nanoscale dimensions, including realizing the ability to restrict light propagation to specific directions, providing the sub-diffractional equivalent of Fabry-Perot cavities, and offering frequency-dependent polariton propagation rotation. In this Perspective, we first discuss the physics behind polaritons supported by anisotropic materials, moving to highlight recent advances in naturally anisotropic polaritonic materials, hybrid materials, and their influence upon the field of infrared nanophotonics. We conclude with an overview of existing challenges that remain for the field before such opportunities can be truly exploited for advanced nanophotonic concepts and devices.

Theories of Polariton Anisotropy

While highly anisotropic crystals have been employed in optics for a broad array of functions, it has only been in the last two decades that extreme forms of anisotropy have been explored for light confinement and subdiffractional manipulation and collection. One phenomenon in this vein is hyperbolicity, as described above. Highly reflective materials such as metals in the visible spectral range are mathematically defined by $Re(\varepsilon) < 0$, while more traditional refractive dielectrics have a positive permittivity. Therefore, hyperbolic media can be considered as a material exhibiting metallic and dielectric optical properties simultaneously at the frequencies of interest.

Probing polaritons: Prior to describing polaritonic modes in isotropic and anisotropic media, we briefly introduce the approaches to probe polaritons, as these optical modes exhibit high-momenta that cannot be directly excited and probed via free space. The probing of surface-bound and hyperbolic polaritons stressed in this Perspective can be realized in both the near- and far-field. In the near-field, they can be measured directly via scattering-type scanning near-field optical microscopy (s-SNOM) and/or a similar technique referred to as nano-FTIR, allowing the user to acquire information on the local photonic density

of states.[26–28] Technical details of these metrologies can be found in several reviews.[29,30] Both techniques employ a metal-coated atomic-force microscope (AFM) tip close to the material surface (~10-70 nm) to scatter the incident light, enabling the excitation and detection of the supported high momentum signal (here polaritonic response) to be collected. As such, the tip itself behaves as an excitation (scatters light into high momentum polaritons) and detection point (collects high momentum light, *e.g.,* polaritons) simultaneously. However, for polaritons probed within slabs of two dimensional materials, interference effects must be exploited for them to be observed, thus they cannot be observed in pristine and infinitely large hyperbolic media via these techniques. To observe propagating polaritons, a second scattering object must be included to induce the interference effect. The most common ways are:[31] (1) relying on a physical edge of the polariton supporting material to realize tip- and/or edge-launched polaritons; (2) creating a dielectric environment difference under and/or above the 2D polaritonic medium or (3) providing a highly scattering object such as a metal nanostructure. These methodologies have been thoroughly studied with the launching efficiencies found to vary between the different methods.[31,32] Note that s-SNOM can also be used to directly probe the propagation of polaritons (*i.e.* with no tip-induced excitation) by employing a dielectric (typically silicon) AFM tip.[33,34] In this case, polaritonic nanostructures with enhanced LDOS, such as resonant nanoantennas,[33] are used as polaritonic sources. In the far-field hyperbolic polaritons can be launched via Mie scattering of patterned antennae,[8,35–39] scattering off of periodically patterned gratings,[40–43] or evanescent coupling through a high index prism[44–47] in either the Otto or Kretschmann configuration. These approaches have the primary advantage that they allow coupling to highly specific wavevectors of light, while losing the ability to spatially resolve the local density of photonic states. Thus, one can interpret near-field techniques as operating in the spatial, with far-field measurements operating in the momentum domain. However, it is important to note that modes in nanostructured films are no longer the exact same electromagnetic modes excited in planar films. Importantly, the photonic bands can be formed and/or altered when the hBN and/or the underlying structure is patterned, and the (sub-diffractional) photonic crystals have been studied in both infrared (polaritonic)[48–52] and visible (dielectric).[53] The choice of technique to probe a hyperbolic polariton therefore depends on whether it is more critical to accurately determine the spatial or momentum information from the system.

Isotropic media and surface polaritons: To appreciate the implications of hyperbolic materials, the benefits afforded by surface polaritons must first be presented. For light in an isotropic dielectric (e.g., air), the wavelength follows the well-known $\hbar\omega = hc\sqrt{\varepsilon}/\lambda_{FS} = \hbar c\sqrt{\varepsilon}|k_{FS}|$, where ω and k_{FS} represent the incident frequency and the wavevector (momentum) of light in free-space (see green line, **Fig. 1a-c**).

We note that this propagation can occur in any direction at a given frequency, which can be represented through plotting the possible wavevectors allowed for propagation in the form of an iso-frequency surface in wavevector space, as shown in **Fig 1d**. For isotropic materials exhibiting a negative real part of the permittivity, strong coupling between light and matter causes a splitting of the dispersion relation, leading to a bulk polariton gap, which we represent in **Fig. 1a** for a phonon polariton material where SPhPs can be supported between transversal (TO) and longitudinal optic (LO) phonon frequencies in a region called the Reststrahlen band.[2,5,54] Optical modes can be supported in this forbidden band provided part of the energy does not reside inside the polaritonic material; that is the mode exists as an evanescent field confined to the surface or interface with an adjacent dielectric.[55] As this results from strong coupling between light and coherent charges, surface polaritons behave light-like at lower frequencies, as indicated by the coincidence of the light-line with the polaritonic dispersion (see **Fig. 1a**, where the green and black curves converge near red dashed line) transitioning to higher momenta (shorter wavelengths) associated with a more charge-like response as the frequency increases (black curve towards blue dashed line **Fig. 1a**). Polaritons exist in many forms,[56] including (but not limited to) SPhPs (**Fig. 1a**),[2,5] SPPs,[55] exciton,[3,4,57,58] Cooper-pair,[3] magnon[3,59–61], Landau,[62–64] vibrational,[65–68] and molecular polaritons,[69–71] yet for this article we will confine our focus to PhPs and PPs.

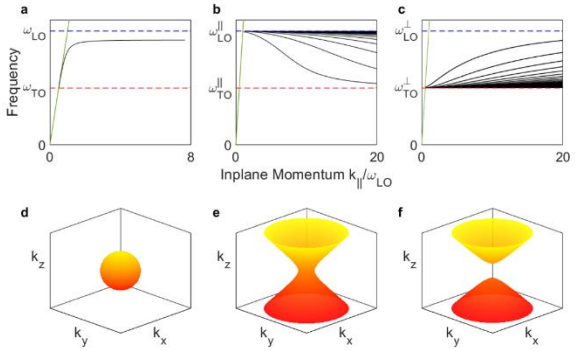

Fig. 1. Isotropic and Hyperbolic Phonon Polaritons. *Generic dispersion of a) isotropic SPhPs, b) type-I volume-confined HPhPs, and c) type-II volume-confined HPhPs. Corresponding d) isotropic and e) type I and f) type II hyperbolic isofrequency contours.*

Uniaxial Hyperbolicity: In a uniaxial hyperbolic medium, two of the crystal axes have an identical dielectric function, with the third exhibiting a dielectric permittivity tensor that is opposite in sign. Thus, light propagation in hyperbolic media is different from that within either isotropic dielectrics or isotropic polaritonic materials. As the permittivity along at least one material axis is negative, polaritons can be supported and light can be confined to sub-diffractional dimensions. However, unlike surface polaritons, the positive permittivity along the other axis (axes) ensures polaritons can still propagate within the *volume* of the hyperbolic media, leading to sub-diffractional volumetric confinement of light.[6,8,72] In further contrast to isotropic polaritonic media, hyperbolic materials can support almost arbitrary, thickness-dependent wavevectors of polaritonic modes with increasing momenta (decreasing wavelength) simultaneously, giving rise to ray-like propagation. Yet, this extended range of accessible momenta comes at the 'cost' of a restriction in the propagation to a frequency-dependent fixed angle, as can be parameterized by calculating the possible wave vectors

supported at a fixed frequency (so called iso-frequency contours). These are found most easily in a material with an arbitrary dielectric tensor $\boldsymbol{\varepsilon}$ by considering light with fixed frequency of wavevector $\underline{\boldsymbol{k}} = n\underline{\boldsymbol{k_0}}$ with a direction defined by a real vector $\underline{\boldsymbol{k_0}} = \frac{2\pi}{\lambda}(\eta_x\underline{\hat{\boldsymbol{x}}} + \eta_y\underline{\hat{\boldsymbol{y}}} + \eta_z\underline{\hat{\boldsymbol{z}}})$ where, $\eta_x^2 + \eta_y^2 + \eta_z^2 = \mathbf{1}$, and a complex refractive index *n*. By finding the determinant of the matrix:

$$\begin{vmatrix} \varepsilon_{xx} + n^2(\eta_x^2 - 1) & \varepsilon_{xy}\eta_x\eta_y & \varepsilon_{xz}\eta_x\eta_z \\ \varepsilon_{xy}\eta_x\eta_y & \varepsilon_{yy} + n^2(\eta_y^2 - 1) & \varepsilon_{yz}\eta_y\eta_z \\ \varepsilon_{xz}\eta_x\eta_z & \varepsilon_{yz}\eta_y\eta_z & \varepsilon_{zz} + n^2(\eta_z^2 - 1) \end{vmatrix} = 0,$$

it is possible to find the complex wave vectors of light in different propagation directions.[73,74] In the limit of high photon wavevectors in a uniaxial material this can be generalized to $tan(\theta) \propto \sqrt{\varepsilon_t/\varepsilon_{zz}}\, i$, for a material where the in-plane transverse permittivities are equivalent $(\varepsilon_t = \varepsilon_{xx} = \varepsilon_{yy})$, the out-of-plane ($\varepsilon_{zz}$) is different and opposite in sign, all off-diagonal elements are zero and with i representing the imaginary unit.[72,75] In finite thickness slabs, the restricted angle of propagation dictates a defined path-length inside the material, resulting in specific conditions where the pathlength is a multiple of one of the series of compressed $\lambda_P s$, leading to a series of standing polaritonic waves with the supported wavevectors written as:[9]

$$k(w) = k' + ik'' = -\frac{\psi}{d}\left[\operatorname{atan}\left(\frac{\varepsilon_o}{\varepsilon_t\psi}\right) + \operatorname{atan}\left(\frac{\varepsilon_s}{\varepsilon_t\psi}\right) + \pi l\right], \quad \psi = -i\sqrt{\frac{\varepsilon_{zz}}{\varepsilon_t}} \tag{1}$$

where *d* is the thickness, ε_o, ε_s are the complex dielectric functions of air, the substrate, respectively, and *l* is the modal order (*l*=0 here). This implies that hyperbolic media behave like a sub-diffractional Fabry-Perot cavity, with multiple branches in the polaritonic dispersion that each exhibit a progressively reduced λ_P (**Fig. 1b**, and **c**). The behavior depends on which axis (axes) is negative, with the most common forms being the Type I (one axis exhibits negative permittivity, typically z; **Fig. 1b, e**) and Type II (two axes negative, typically $x = y$; **Fig. 1c, f**). However, it has been challenging to observe such ray-like propagation directly, as hyperbolic materials typically exhibit this behavior in out-of-plane directions that are difficult to experimentally probe. Yet, using hexagonal boron nitride (hBN) frustums (truncated cones), the ray-like propagation was directly confirmed by employing scattering-type scanning near-field scanning optical microscopy (s-SNOM) along the sloped sidewalls.[75] This material is a two-dimensional van der Waals crystal similar to graphene/graphite in structure[72] that serves as an exemplary natural hyperbolic material supporting hyperbolic phonon polaritons (HPhPs) in two spectrally distinct Reststrahlen bands[54] (RBs). The lower frequency RB is type I (**Fig. 1b,e**) and is observed λ_{FS}~12.1-13.2 μm (**Fig. 2a**, pink region), while the

upper is type II (**Fig. 1c,f**) and occurs within λ_{FS}~6.2-7.3 μm (**Fig. 2a**, green region).[8,9] Similarly, the demonstration of natural hyperbolicity was also reported in quartz[10] and calcite,[76] among an ever-growing list.[4,11,77] Notably, HPhP modes would strongly increase the local density of photonic states due to the coupling to high-k modes.[78]

Biaxial hyperbolicity: Analogous to uniaxial hyperbolicity, biaxial hyperbolicity occurs within materials where $Re(\varepsilon)$ values are different, but this holds for all three crystal axes, with one being opposite in sign to the others. As such, these materials can show type I and type II hyperbolic bands that exhibit momenta dependent upon the direction of propagation. Therefore, these materials will be inherently more dispersive in terms of their waveguiding properties. Due to the varying properties of each of the crystal axes, in-plane hyperbolic behavior and ray-like propagation are more easily observed in biaxial hyperbolic materials.[15] Furthermore, this allows for controlling polarization more easily, even at near-normal incidence,[79] versus only being readily accessible at high angles for uniaxial materials with the optical axis normal to the surface, as in hBN.[80] An exemplary material in this regard is MoO_3,[14,81,82] whereby the anisotropic optic phonons along the three principal axes give rise to multiple RBs (Fig. 2b) where polariton

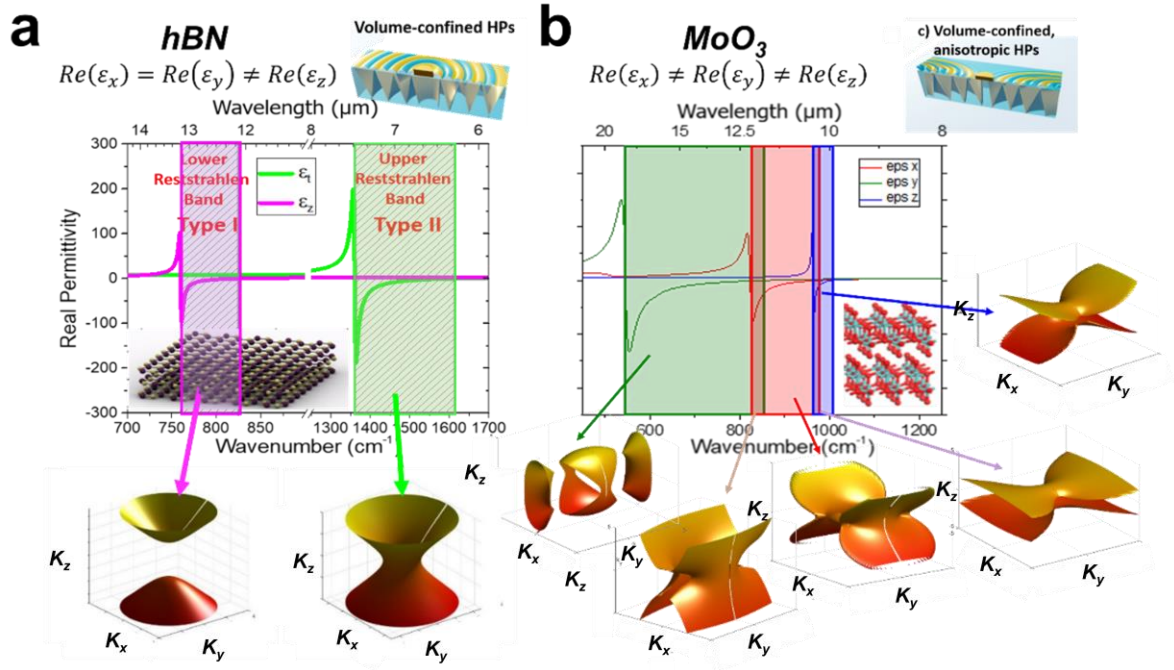

Fig. 2: Isofrequency contour of exemplary hyperbolic materials. *a) hBN supports uniaxial hyperbolicity, and HPhPs are isotropic in the x-y plane. b) The dielectric function of α-MoO3 exhibits different values along different crystal directions, supporting biaxial hyperbolicity. In-plane and elliptical HPhPs are supported in different frequency ranges. Isofrequency contours representative of the specific spectral ranges where hyperbolicity is observed are provided for both materials. Panel a is adapted with permission from reference [8]. Copyright 2014 Nature Publishing Group. Panel b is adapted with permission from reference [82]. Copyright 2020 John Wiley & Sons, Inc.*

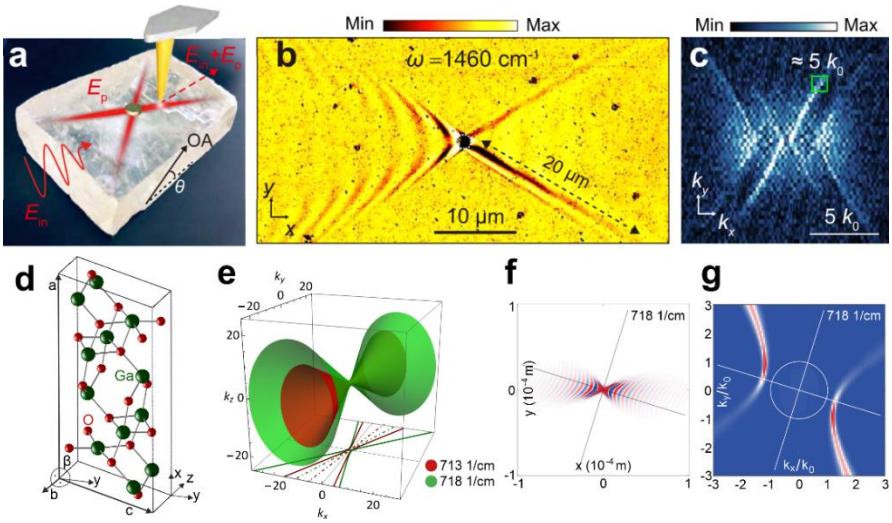

Fig. 3 Off-cut and lower symmetry hyperbolicity. *(a-c) Ghost hyperbolic polaritons supported by off-cut calcite crystal. a) measurement schematic; b) Experimental s-SNOM measurement of ghost polaritons; c) Absolute value of the Fourier transform of the image shown in panel b); d-g) Shear polaritons supported by β-Ga_2O_3. d) Crystal structure of monoclinic β-Ga_2O_3; e) isofrequency surface of β-Ga_2O_3; Calculated fields of: f) Real-space electric fields at the β-Ga_2O_3 surface; g) The two-dimensional Fourier transformation of panel f). Panel a-c are reprinted with permission from reference [17]. Copyright 2021 Springer Nature. Panel d-g are reprinted with permission from reference [18]. Copyright 2022. Springer Nature, licensed under a Creative Commons Attribution (CC BY) license: : https://creativecommons.org/licenses/by/4.0/.*

propagation can be supported as designated by the overlayed shaded regions in the dielectric function of MoO_3.[80,82] For instance, within the blue region, only the out of plane permittivity tensor is negative, giving rise to a similar hyperbolic response to that of the upper RB of hBN, albeit with the polaritonic waves propagating along the x and y directions exhibiting different λ_P s. However, in the red and green shaded regions the x- and y-axes permittivities become negative, respectively, giving rise to in-plane hyperbolicity; that is, the polariton propagation is restricted to the condition: $\left|\tan\left(k_{xx}/k_{yy}\right)\right| < \sqrt{\left(\varepsilon_{yy}/\varepsilon_{xx}\right)}/i$ (see cross-sectional schematic in upper right, **Fig. 2b**), which stands in stark contrast to the isotropic in-plane propagation of hyperbolic polaritons in hBN (top right, **Fig. 2a**). Additional regimes where these bands overlap (purple arrow, yellow arrow in **Fig. 2b**) result in even more complicated hyperbolic propagation as evidence by the representative isofrequency contours for each of these regimes (**Fig. 2b**).

Off-cut and lower symmetry hyperbolicity: When studying hyperbolic materials, it is often convenient to operate with the optical axes of the crystal aligned with the coordinate system in the laboratory. This allows for an easier definition of the dielectric properties of materials, as well as easing the understanding of any surface- or volume-confined waves. However, in both uniaxial (*e.g.* calcite) and biaxial materials it is possible to produce crystal off-cuts where the crystal axes are misaligned with the surface (**Fig. 3a**). This

is also common in various silicon carbide polytypes as the off-cuts are used to induce step-wise epitaxial growth,[83] as well as for sapphire, where multiple off-cuts are commercially available for improved lattice

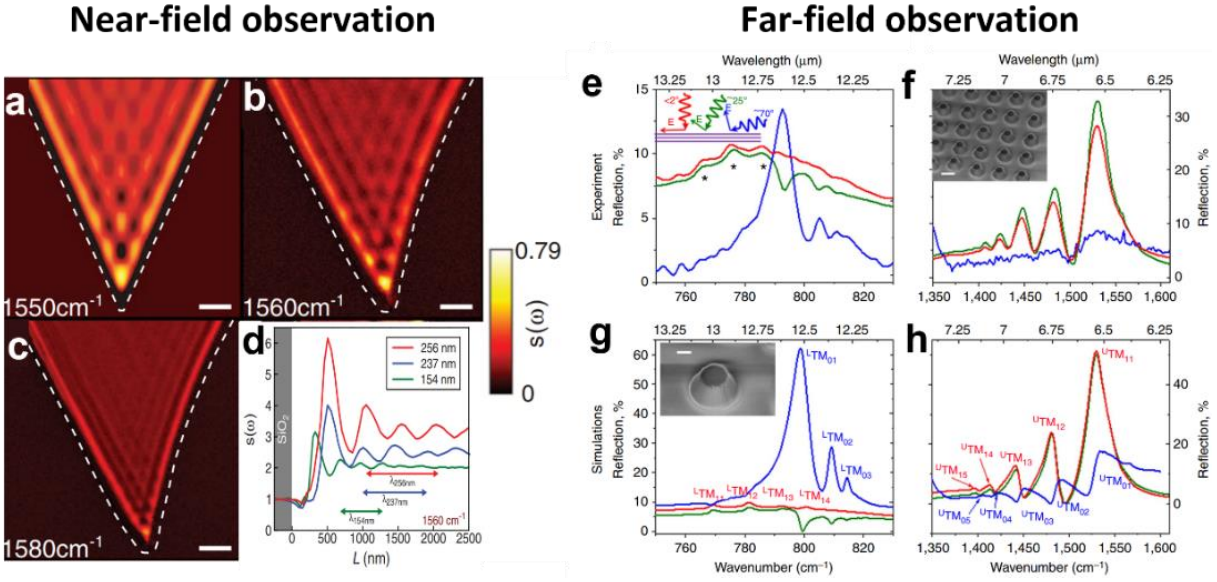

Fig. 4 Experimentally observed hyperbolic phonon polaritons supported by hBN*. a-c) Experimentally observed propagating HPhPs supported in a hBN slab in the near-field via s-SNOM. At different frequencies, the polariton wavelength varies, dictated by Eq. (1). d) Linescans extracted from s-SNOM measurements on variable thickness hBN are provided, from which the HPhP wavelength at 1560 cm^{-1} was extracted. e-h) High-order HPhP modes supported by nanostructured hBN are observed in the far-field from frustums fabricated into hBN flakes (inset SEM). Experimental and simulated spectra within the lower and upper Reststrahlen bands of hBN are provided and demonstrate that the higher order modes can be directly excited from the far-field. Panel a-d are apated with permission from Reference [9]. Copyright 2014 AAAS. Panel e-h are reprinted with permission from Reference [8]. Copyright 2014 Nature Publishing Group.*

match for heteroepitaxy. In such off-cut, anisotropic crystals one can support so-called 'Ghost polaritons', which are defined as those that are partially evanescent and propagating waves in character.[17] The formation of polariton rays can be explained by the larger local photonic density of states. Experimentally, the polaritons can be observed via s-SNOM measurements on off-cut calcite surfaces (**Fig. 3b**), with the resultant momentum-space plots extracted via Fourier transforms (**Fig. 3c**). Hyperbolicity can also arise from crystals with further reduced symmetry, such as those featuring monoclinic (**Fig. 3d** for β-phase Ga_2O_3) and triclinic Bravais lattices, where the non-orthogonal nature of at least one of the principal crystal axes leads to a permittivity tensor matrix that cannot be diagonalized. Such low crystal symmetry gives rise to a shear force applied to the hyperbolic polaritons supported, resulting in so-called 'shear polaritons' where the propagation direction is found to rotate in the plane as the incident frequency is modified within a given RB (**Fig. 3e-f**).[18] The Fourier transform of **Fig. 3f** illustrates such a frequency-dependent rotation as well as the strong anisotropy in the momentum space plot (**Fig. 3g**).

Materials for Polariton Anisotropy

From Artificial to Natural Uniaxial Hyperbolic Materials: Originally, hyperbolic behavior was investigated using artificial hyperbolic metamaterials (HMMs)[6,78,84,85] featuring alternating sub-wavelength scale metal and dielectric domains, with the hyperbolic behavior well-described by the effective medium approximation.[86] While many novel physical phenomena have been reported using such systems, including negative refraction,[87–92] hyperlensing,[93–97] and subdiffractional-lithography,[98,99] the high optical losses resulting from the metal elements[100–102] severely restricts their use beyond the laboratory. However, in 2012 and 2014 hyperbolic behavior was reported for the first time in the naturally anisotropic crystals quartz[10] and hexagonal boron nitride (hBN),[8,9] respectively. In the case of the latter, the seminal works of Dai et. al[9] demonstrated the thickness-dependent dispersion of hyperbolic modes (**Fig. 4a-d**), indicating that $\lambda_P(\omega)$ changes as a function of slab thickness, while Caldwell et al.[8] experimentally confirmed that multiple higher-order HPhP modes could be supported simultaneously within nanostructures (**Fig. 4e-h**), giving rise to multiple resonant conditions with progressively decreasing λ_P. Later work by Giles et al.[103] employed isotopically enriched hBN to enable the direct observation of these higher-order HPhPs propagating simultaneously at a fixed incident frequency using s-SNOM, with such modes previously only observed via Fourier transforms of s-SNOM linescans near hBN flake edges.[97] Note that monolayer hBN can also support ultra-high momentum HPhPs.[104–106] The optic phonon origin of the HPhPs significantly reduced the optical losses in contrast to previously reported HMMs, resulting in

significant improvements in hyperlens imaging resolution,[96,97,107] Q-factors[8,108] and propagation lengths.[9,37,103,109–111]

From Artificial to Natural Biaxial Hyperbolic Materials: Beyond hBN, a whole host of natural hyperbolic materials have been identified.[4,11,72,77] However, extending beyond the simplified type I and II HPhPs supported in hBN, the realization of in-plane hyperbolicity ($Re(\varepsilon) < 0$ along one in-plane direction, while it is $Re(\varepsilon) > 0$ along the other) promises significant opportunities[79] by enabling the restriction of propagation to a single in-plane direction,[13,14,81] as highlighted above for MoO_3. Again, such so-called 'in-plane hyperbolicity' was initially demonstrated in HMMs,[112] and was later identified in hBN patterned into strips via focused ion beam (FIB),[13] as shown in **Fig. 5a**. Thus, in this structured system the polaritonic wavefront is launched via scattering off a metal antenna (**Fig. 5a-c**) and was directionally propagated parallel to the hBN stripes (here perpendicular to the gold antenna tip). However, in 2018 such in-plane hyperbolic response was observed within the natural crystal MoO_3.[14,81] Here using s-SNOM again, but on unpatterned crystals of MoO_3, the same highly directional propagation of HPhPs was observed within in-plane hyperbolic bands (**Fig. 5d and f**), while in others where the two in-plane bands are of the same sign, but different magnitudes, where polaritonic waves are observed to propagate in both directions, albeit with distinctly different λ_P (**Fig. 5e**, 'elliptical band').

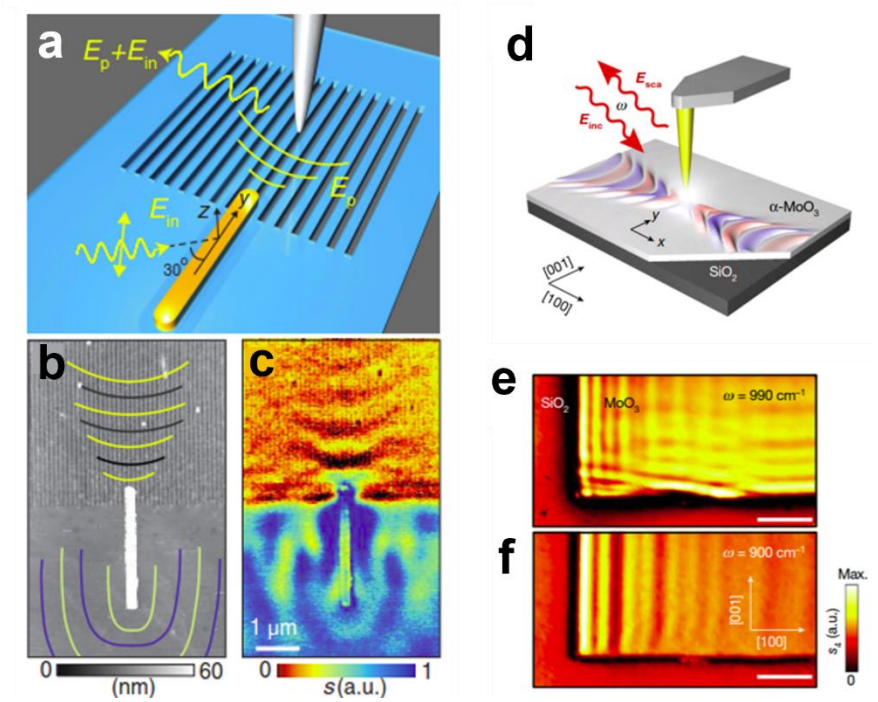

Fig. 5 Artificial and natural biaxial hyperbolic materials*. a) Patterned hBN nano-structure shows in-plane hyperbolicity, resulting from effective media effect (hBN/air alternating layers). b, c) The in-plane hyperbolicity is confirmed by s-SNOM measurement. d) Natural in-plane hyperbolic material (MoO_3). e) HPhPs are both supported in [001] and [100] crystal directions at 990 cm^{-1}, albeit with different polariton wavelength (elliptical band). f) At the in-plane hyperbolic range, e.g., 900 cm^{-1}, only HPhPs along [100] crystal direction are allowed. Panel a-c are adapted with permission from reference [13]. Copyright 2018 AAAS. Panel d-f are adapted with permission from reference [14]. Copyright 2018 Springer Nature.*

While prior calculations and measurements of MoO_3 had been employed to extract an approximate uniaxial dielectric function, it was through correlated far-field Fourier-transform infrared spectroscopy (FTIR) and near-field s-SNOM measurements that the quantification of the IR dielectric function of this material was extracted (**Fig. 2b**),[82] with these results validating the previously measured s-SNOM and nano-FTIR experiments within the three RBs of the material (**Fig. 5d-f**). Such directional propagation is further extended to non-symmetric cases within calcite[17] and β-Ga_2O_3[18] that have been recently shown to exhibit the more exotic forms of polaritons discussed above.

From Static to Dynamic Hyperbolic Materials: Despite an increasing array of anisotropic and hyperbolic materials, single materials often limit the engineering control and frequency tuning of the supported polaritonic modes. Dynamic tuning of HPhPs is especially problematic, as these modes arise from the lattice vibrations of a polar material and are inherently fixed in frequency for a given material composition. For instance, while hBN offers high Q-factor resonances and long propagating HPhPs, the large bandgap (~5.95 eV)[113,114] precludes free-carrier injection for active modulation as has been demonstrated for SiC, InP, and GaN,[115–117] therefore requiring external stimuli to the surrounding medium to induce any changes in polaritonic response.[118,119] Recently, Taboada-Gutiérrez et al.[16] demonstrated frequency tuning of the hyperbolicity in V_2O_5 by sodium intercalation, thereby providing significantly greater flexibility via a hybrid material approach (**Fig. 6a-d**). In addition, hyperbolic Rydberg polaritons, which may be formed in transitions of excitons between states with differing quantum numbers coupled to photons, can be turned on and off at picosecond time scales in WS_2 slabs (**Fig. 6e, f**), as demonstrated by Sternbac et. al.[120] Yet, such approaches still represent material-specific opportunities rather than general approaches to dynamic tuning appropriate for any HPhP-supporting material, and thus additional solutions to this challenge must also be identified.

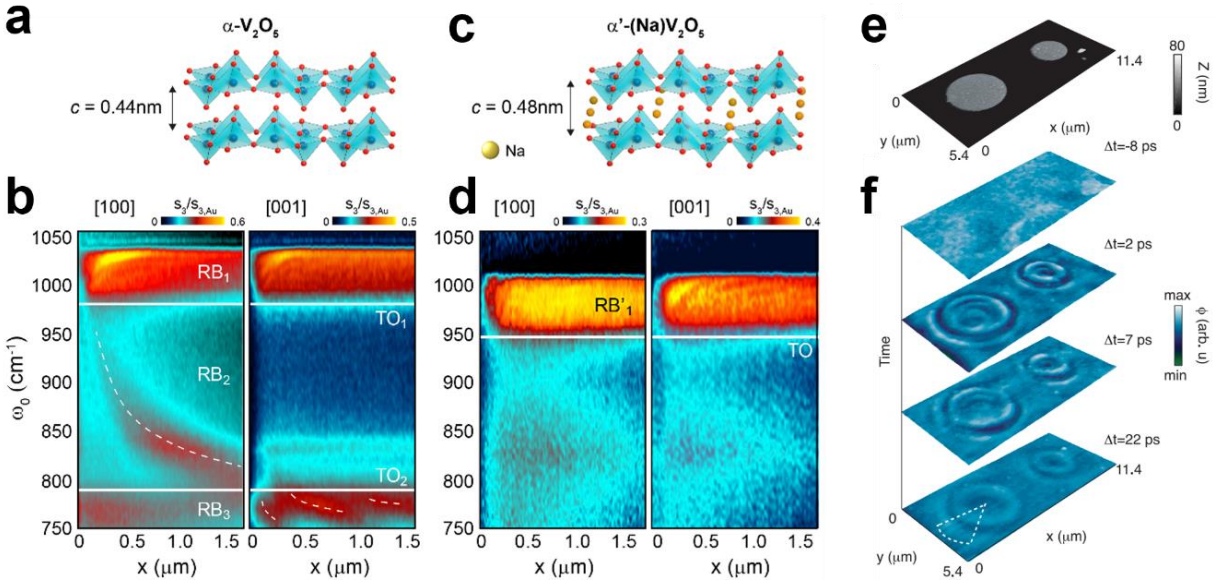

Fig. 6 Dynamic hyperbolic materials*. a,b) The HPhP response supported by α-V_2O_5 can be c,d) spectrally tuned by Na^+ intercalation.*[16] *The a) crystal structure of the pristine α-V_2O_5 and corresponding b) nano-FTIR measurements along two crystal directions are presented without any intercalation, showing the natural in-plane hyperbolicity within RB2. After Na+ intercalation, c) the lattice expands causing d) the RB1 is shifted to lower frequency, while RB2 is no longer observed. e,f) The transient hyperbolic Rydberg polaritons are supported by WSe_2 when photo-injected carriers are at a sufficient level.*[120] *Panel a-d are reprinted with permission from reference [16]. Copyright 2020 Springer Nature. Panel e-f are reprinted with permission from reference [120]. Copyright 2021 AAAS.*

Engineering Polariton Anisotropy through Hybrid Materials

The significant opportunities in nanophotonics afforded by material anisotropy can be further expanded by artificially engineering the polaritons supported. In the context of dynamic tuning, such engineering can provide alternative platforms for active control of polaritonic properties through stimuli to the local environment or an adjacent polaritonic material. Two principal methods have been discussed: (1) controlling/modifying the local environment[118,119,121] and (2) coupling between different polaritonic modes in adjacent materials.[45,122–126] However, such hybridization concepts have also been exploited to completely modify the dielectric function of materials through the (3) crystalline hybrid concept that can be realized through atomic-layer superlattice design.[20,22]

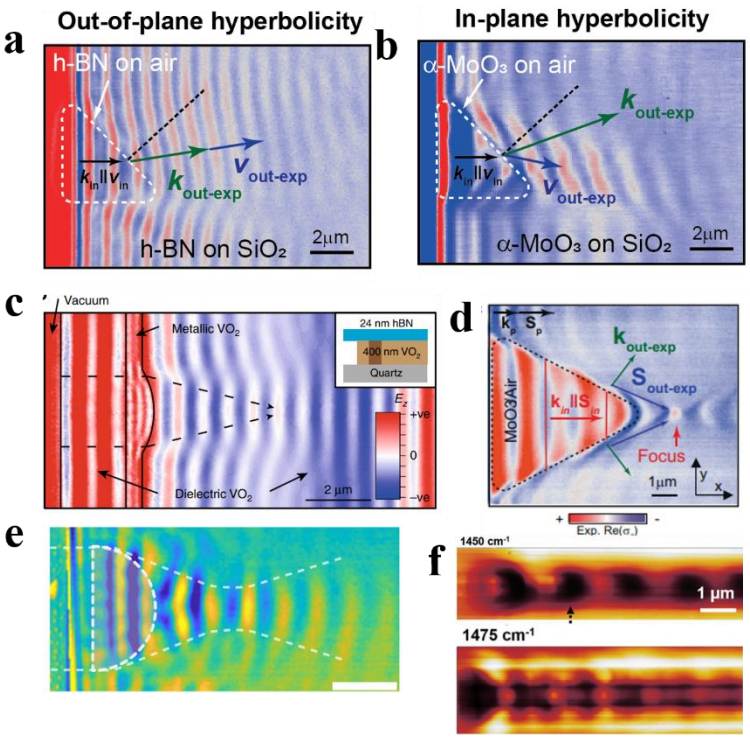

Fig. 7. Engineering polariton propagations via polaritonic refractions. *a) Manipulation of in-plane isotropic HPhPs in hBN via local environment. Refraction takes place under the most conventional form of Snell's law. b) Manipulation of in-plane hyperbolic HPhPs in MoO_3 via the same approach. Refraction gives rise to non-intuitive directions of propagation of both wavevector k and Poynting vector S. c, d) In-plane lens formed by underlying patterns. e, f) In-plane lens and waveguides of HPhPs formed by the underlying patterns. Panel a,b and d are adapted with permission from reference [133] (with changes). Copyright 2021 Springer Nature, licensed under a Creative Commons Attribution (CC BY) license: : https://creativecommons.org/licenses/by/4.0/. Panel c is reprinted with permission from reference [118] (no changes). Copyright 2018 Springer Nature, licensed under a Creative Commons Attribution (CC BY) license: https://creativecommons.org/licenses/by/4.0/. Panel e is reprinted with permission from reference [121] (no changes). Copyright 2019 Springer Nature, licensed under a Creative Commons Attribution (CC BY) license: https://creativecommons.org/licenses/by/4.0/. Panel f is reprinted with permission from reference [134]. Copyright 2021 John Wiley & Sons, Inc.*

Controlling the Local Environment: The first method towards engineering polaritonic properties is based on controlling the local environment. While broadly implemented for various SPP-based concepts, including the ubiquitous surface plasmon resonance (SPR) biosensing scheme,[127–129] the volume-confined nature of HPhPs implied a more limited influence upon the local environment.[8] However, recent experiments have demonstrated that such hyperbolic modes indeed remain sensitive to the local refractive index, as shown in Eq. (1). It has been experimentally demonstrated that HPhPs supported by hBN over materials of various refractive indices exhibit different wavevectors[119] and thus, different λ_Ps, and the propagation within a given slab of a hyperbolic material over a domain between two different dielectric environments results in in-plane refraction.[118] In the case of HPhPs in hBN, due to their in-plane isotropic propagation, refraction occurs under the most common expression of Snell's law (**Fig. 7a**), *i.e.,* the waves bend towards the normal to the boundary when passing from a low- (inside white dashed triangular area in **Fig. 7a**: hBN/air) to a high-refractive index (outside white dashed triangular area in **Fig. 7a**: hBN/SiO_2) medium. However, in the case of in-plane HPhPs such as those

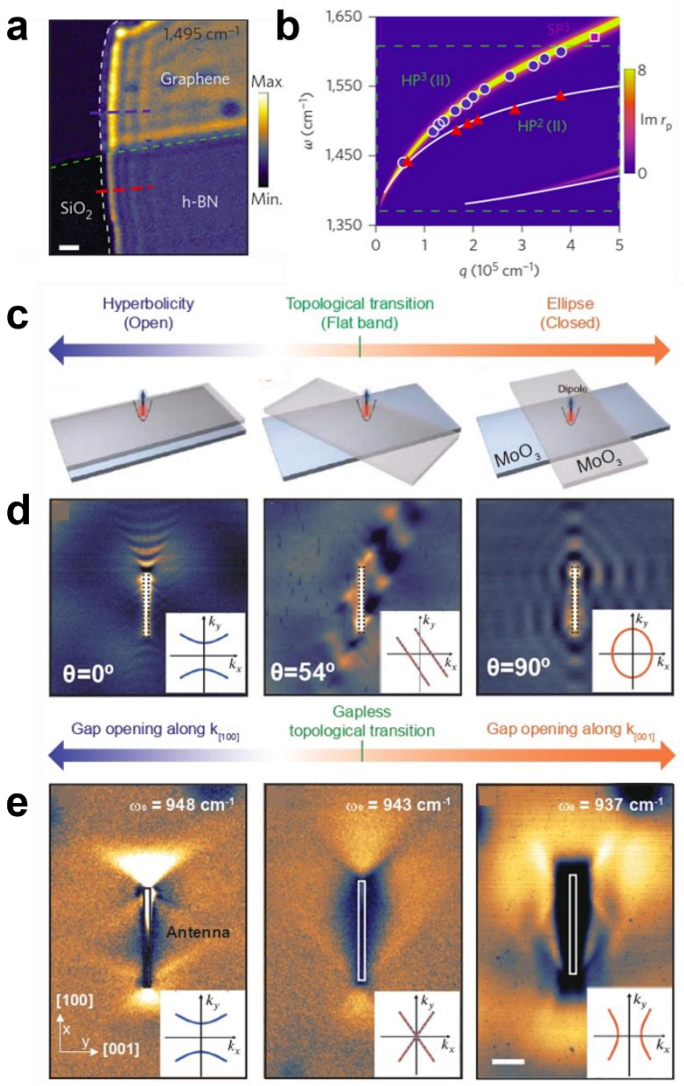

Fig. 8. Engineered in-plane anisotropy of HPhPs by electromagnetic mode coupling. *a, b) The HPhPs supported by hBN (in-plane isotropic) can be coupled to isotropic SPPs supported by graphene, leading to hybridized modes.[19] c, d) Photonic topological transition in twisted bi-layered α-MoO_3: the polaritonic isofrequency curve (IFC) transits from an open hyperbola (left panel) to a closed ellipse (right panel) passing through a "flat band" regime (two parallel lines, middle panel), at which polaritons propagate along one specific direction (canalization regime).[24] e) Photonic topological transition in α-MoO_3/4H-SiC heterostructures: the polaritonic IFC transits from an open hyperbola centered along the [100] crystal direction (left panel) to an open hyperbola centered along the [001] crystal direction (right panel). The transition occurs through a gapless IFC formed by two crossing lines (middle panel). The propagation direction of HPhPs in α-MoO_3 can thus be reverted via mode coupling.[147] Panel a and b are adapted with permission from reference [19]. Copyright 2015 Springer Nature. Panel c and d are adapted with permission from reference[24]. Copyright 2020 American Chemical Society. Panel e is from reference [147]. Copyright The Authors, some rights reserved; exclusive licensee AAAS. Distributed under a CC BY-NC 4.0 license http://creativecommons.org/licenses/by-nc/4.0/". Reprinted with permission from AAAS. The isofrequency curves are added onto the original figure.*

supported in MoO_3, refraction is a more exotic phenomenon,[130] yielding the polaritonic wavevector ($\mathbf{k}_{out\text{-}exp}$) to refract towards the normal while the energy flux bends away from it (**Fig. 7b**).[131,132] This unusual phenomenon has been recently exploited to demonstrate a refractive planar hyperlens (white dashed triangle in **Fig. 7d**), yielding sub-diffractional foci as small as $\sim \lambda_p/6$.[133] These refractive phenomena allow for the deterministic control of the wavelength of the anisotropic modes, thereby providing a path to chemical sensors based on the surface enhanced IR absorption (SEIRA) concept[125] as well as on-chip photonic components, such as waveguides (**Fig. 7f**), lenses (**Fig. 7c, e**) and resonators.[118,121] Furthermore, such an approach was recently demonstrated to provide frequency multiplexing within unpatterned hBN, with the wave propagation dictated by the underlying silicon photonic architecture.[134] However, while such an approach enables direct control of HPhP propagation, and potentially in an active and/or reconfigurable manner,[118,121] this does not inherently provide a methodology to modify or remove the inherent anisotropy of the polaritonic material or modes.

Coupling among different photonic modes: The second approach, which is similar but fundamentally different from the first, is to introduce polaritonic coupling, thereby giving rise to SPP/HPhP, HPhP/HPhP or SPhP/HPhP hybrid modes. Just as strong coupling between a photon and a coherent charge oscillation gives rise to a polariton mode that exhibits hybrid properties of both constituents, polariton-polariton strong coupling offers similar benefits.[135] As originally demonstrated by Woessner et al.,[136] a heterostructure comprised of hBN and graphene enabled the opportunity to significantly extend the lifetimes and propagation lengths of SPPs in graphene in the spectral ranges outside of the RBs of hBN. Subsequent efforts within similar heterostructures by Dai et al.[19] demonstrated that within these bands that SPP-HPhP strong coupling could be induced, which in turn enabled the ability to control the hybrid $\lambda_P$and propagation characteristics through electrostatic gating of the graphene,[137–139] while maintaining the volume-confinement and multiple polariton branches associated with the hBN HPhPs (**Fig. 8a,b**). This approach, later referred to as the electromagnetic hybrid concept,[21] offers significant opportunities for controlling polaritonic properties in lower symmetry materials, as discussed below in the perspectives section. More recent efforts have extended into the realm of polaritonic strong coupling, which has enabled the hybridization of so-called epsilon-near-zero-polaritons (ENZ) and propagating SPPs [124] or SPhPs,[45] enabling the potential to dictate the polaritonic dispersion, including modifying the group velocity, field concentration and polaritonic wavevector. However, in all such approaches only the wavelength of the anisotropic polaritons is directly controlled, yet we envision that similar electromagnetic hybrids can be realized by graphene and biaxial hyperbolic materials in which the polariton propagation direction also changes. For instance, one can potentially change the propagation direction of in-plane hyperbolic polaritons in MoO_3 when a graphene layer is included, while such observations could also be observed by locally changing the carrier density in the vicinity of shear polaritons.

In addition to coupling between isotropic SPPs and anisotropic SPhPs, the coupling between two anisotropic PhP media may also provide significant benefits. Notably, inspired by the discovery of flat-band superconductivity[140] and ferromagnetism[141] in twisted bilayer graphene, it has been reported that stacks of two twisted layers of α-MoO_3 allow further design freedom in engineering the direction of propagation of hybrid HPhP modes, thus introducing an unprecedented degree of control over the manipulation of in-plane anisotropic polaritons through the implementation of the field of 'twist-optics'.[24,142,143] In these works, hybrid HPhPs/HPhPs were demonstrated, showing altered directionality of propagating HPhPs (**Fig. 8c,d**). The images revealed polaritonic isofrequency contours in the hybrid system with different geometries that can be tuned by simply changing the twist angle between the principal

crystalline axis of the stacked individual α-MoO_3 slabs. Remarkably, these isofrequency contours exhibit extreme topological transitions from open hyperbolic-like to closed spherical/elliptical curves, thus having a profound effect on the anisotropic propagation properties of such hybrid modes.[144] Indeed, it was identified that at a critical twist angle, extreme directional propagation of all polaritonic wavevectors along specific in-plane directions emerges – the so-called canalization regime.[145] While this case demonstrated enormous potential for controlling polariton propagation, it does not alter the forbidden propagation direction. By coupling the HPhP with a dielectric-SPhP mode, the allowed (and forbidden) propagation direction can be inverted, which is experimentally demonstrated in the heterostructure of α-MoO_3/SiC (**Fig. 8e**).[146,147] Specifically, it was visualized that the propagation of in-plane HPhPs in α-MoO_3 rotates 90° when the crystal is placed on SiC. Importantly, due to the unique low-loss nature of the topological transition, it was possible to visualize intermediate propagating states, which permits the unveiling of the topological origin of the transition. The general and fundamental character of these findings extends the unique possibilities of twisted polaritons discussed above to develop optical applications requiring propagation of the electromagnetic energy flow along specific directions, *e.g.*, directional coupling between molecules[148] or quantum emitters,[149] or directional thermal management.[150–153]

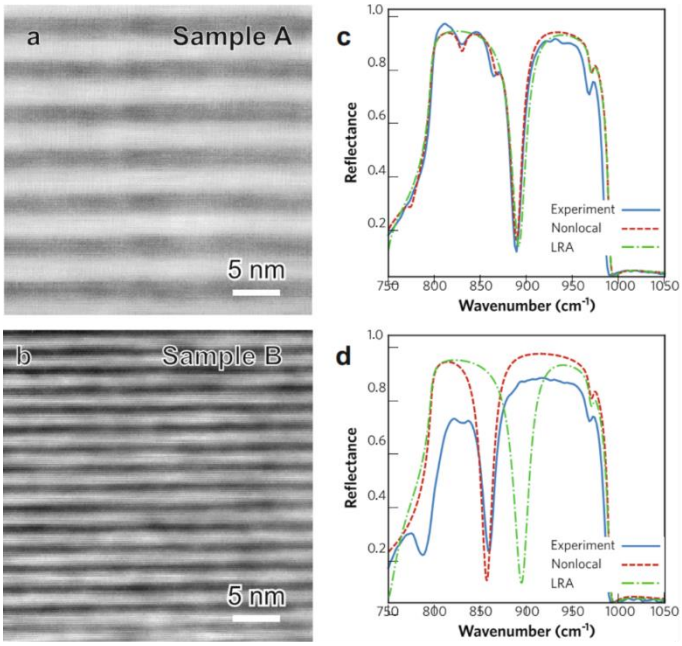

Fig. 9. Non-local effect in crystalline hybrid. *(a, b) Two AlN/GaN atomic-layer superlattices from Ref. [22], with average layer thickness of 2.2nm (Sample A) and 1.3nm (Sample B). (c, d) The reflectance of the two structures as obtained from experiments (blue solid lines), standard (local) dielectric theory (green dash-dotted lines) and using the nonlocal theory from Ref. [23] (red dashed lines). The local theory, neglecting the dispersion of the phonons, fails to reproduce both the position of the main polaritonic resonance and the presence of further ones due to the hybridization with longitudinal modes. Figures are adapted with permission from reference [22]. Copyright 2019 American Chemical Society.*

Crystalline Hybrid: The third concept focuses on manipulating the fundamental atomic structure through atomic-layer superlattice design.[20,21] As the dielectric function within the IR for polar materials is dictated predominantly by the optic phonons, modifications to the fundamental frequencies, scattering lifetimes and/or introduction of new phonon modes will in turn have direct implications upon the IR properties. Such an approach gives rise to the so-called crystalline hybrid concept.[22] Unlike in the above approaches

where we take two relatively thick materials with fixed optical properties and directly couple them, here strongly bonded, atomically thin materials are found to give rise to emergent properties that are different from that of the bulk constituent materials. This is because as the thickness of individual layers within a superlattice are reduced, they approach the length-scale of the optic phonon wavelengths resulting in confinement with modified frequencies at the gamma point within the Brillouin zone.[154–157] Moreover, at such length-scales the approximation of optic phonons as nominally dispersionless (*e.g.,* localized vibrations) fails, and their propagative and dispersive nature becomes important, leading to the appearance of so-called nonlocal phenomena.[23] In addition, the integration of multiple material interfaces with modified chemical bonding offers the potential to introduce new interface phonons, corresponding to vibrational states localized to the interfacial region.[158–160] This has been observed to induce anomalous spectral shifts in localized SPhP resonances due to the introduction of new interface phonons between polar semiconductors and ultrathin dielectrics deposited via ALD.[161] The incorporation of phonon confinement with new interface phonon modes, along with the resulting mixing of longitudinal and transverse charge oscillations, results in frequency shifts and the presence of novel discrete resonances in the far-field spectrum of thin layers as well as the appearance of longitudinal resonances in the local photonic density of states.[23] Yet it is important to note that such nonlocality also increases losses as high-momentum optic phonons can propagate away from the sample, effectively becoming a new loss channel.[23] In all, such modifications result in a fundamentally different dielectric function for this new crystalline hybrid material. These effects have been recently observed by Ratchford et al.[22] within AlN/GaN short-period superlattices (TEM cross-sections in **Fig. 9a,b**), demonstrating a significantly modified IR reflectance (**Fig. 9c, d,** blue curves), and thus, dielectric function and polaritonic dispersion. While *ab-initio* simulations were initially employed to study crystalline hybrids,[22] nonlocal dielectric theories have more recently been shown to correctly reproduce experimental features with limited computational requirements (**Fig. 9c,d**, red curves), making it possible to include nonlocal effects in the design of SPhP devices.[162,163] Further, much like semiconductor quantum wells, this also provides the potential opportunity to inject free carriers in one of the constituents (*e.g*., GaN) to locally tune the SPhPs within the adjacent structure (*e.g.,* AlN) through the electromagnetic hybrid effect.[21] Thus, this could enable opportunities to actively tune polaritonic modes within materials where otherwise such effects are not possible.

Polariton Loss: While polaritons enable strong light-matter interactions through the subdiffractional confinement of light, it comes at the cost of increased losses. Although PhPs possess significantly reduced loss compared with plasmonic counterparts, the loss is still a limiting factor for many applications, for

instance chip-scale communications. To discuss the implications of these losses upon anisotropic polaritons, we first summarize the phonon lifetimes of several highlighted materials including hBN, MoO_3, V_2O_5 and calcite, as shown in **Table 1**. Besides the intrinsic properties, the polariton modes supported by those materials are more critical for applications. Thus, we employ an analytical solution (eq. 1) to find the complex valued wavevectors of hyperbolic modes supported by 20-nm thick slabs of those materials. Additionally, the Q factor offers an indication of the loss-induced limitation on polariton propagation and is defined as $\frac{real\ (k)}{imag(k)} = 4\pi N$, where *N* defines the number of cycles that the HPhPs propagate until the electric field intensity decays to 1/e, with the comparison of the Q factors for these materials provided in **Fig. 10a**. Similarly, the propagation length, $L_p = \frac{1}{imag(k)}$, defines the distance the mode will propagate until the amplitude of the electric field, which can be directly measured in s-SNOM, decays to 1/e.[16] In general, the polariton propagation lengths are limited to the micron scale, which is orders of magnitude below that of refractive optics, as shown in **Fig. 10b**. However, polaritons provide the strong light-matter interactions and high confinement that dielectric materials cannot, thereby enabling significant benefits for sensing applications, compact nanophotonic- and/or metamaterial-based optics, as well as in nanoscale control of light propagation. We further calculated the polariton lifetime by $\tau = L_p/v_g$, where $v_g = \frac{\partial w}{\partial k}$ is the group velocity (**Fig. 10c**). Note that the polariton lifetimes are not equivalent to phonon lifetimes, due to differences in the group velocity (dispersion).

From these comparisons one can derive some insights into how to decrease the loss of polaritons. The most obvious approach is to improve the material quality, e.g., reducing the atomic impurities. For instance, isotopically enriched hBN has exhibited optic phonon lifetimes that are three-to-four times longer than the naturally abundant form (20% ^{10}B, 80% ^{11}B, **Fig. 10 a-c**).[103,164] These improvements come from the suppressed isotopic mass-based scattering, while similar improvements are expected from reduced impurities. As such, it is expected that further materials engineering could improve the Q-factors of anisotropic polaritons, especially for materials with significant isotropic impurities, *e.g.*, MoO_3. Beyond such traditional approaches, mode engineering could also decrease the loss of polaritons. Confinement of a mode is typically negatively correlated with propagation length. For instance, for a given material (99% ^{10}B hBN here), λ_p of the HPhP mode is reciprocal to the material thickness, and thicker hBN (lower confinement) leads to longer propagation lengths and higher group velocities (**Fig. 10d**). It should be noted that the polariton lifetime does not change with thickness in this scenario. In addition to HPhP modes, unique anisotropic polaritons supported by off-cut crystals could also provide significant opportunities in

loss engineering, such as observed for ghost polaritons supported by off-cut calcite which reveals long propagation lengths upwards of 20 μm. Similarly, the confinement of ghost polaritons is weaker than volume-confined modes in thin slabs, leading to longer propagation length. Thus, engineering the dispersion and specifically the magnitude of the confinement allows for additionally tuning of the propagation lengths to meet the requirements of a specific application. It was recently demonstrated that photonic modes supported by silicon photonic crystals could be hybridized with PhP modes, featuring unidirectional propagation with over 80 um propagation distances.[52]

Table 1. Phonon lifetimes of different materials (crystal directions). Phonon frequencies are TO and LO frequencies along the corresponding crystal axis. Phonon lifetimes are derived from the phonon damping, which is extracted from dielectric function fittings.

Material	**Phonon frequencies (ω_{TO}/ω_{LO} cm^{-1})**	**Phonon damping (cm^{-1})**	**Phonon lifetime (ps)**
α-V_2O_5 [001][16]	474.4/815.6	9.6	0.55
α-MO_3 [100][82]	821/963	6.0	0.88
α-MO_3 [001][82]	544/850	9.5	0.56
Natural hBN in-plane[8]	1360/1614	7	0.76
^{11}B 99% hBN in-plane[103]	1359.8/1608.7	2.1	2.5
^{10}B 99% hBN in-plane[103]	1394.5/1650	1.8	2.9

Natural hBN out-of-plane[8]	760/825	3	1.8
^{11}B 99% hBN out-of-plane[103]	755/814	1	5.3
^{10}B 99% hBN out-of-plane[103]	785/845	1.0	5.3
Calcite [100][17,165]	1410/1550	10	0.53

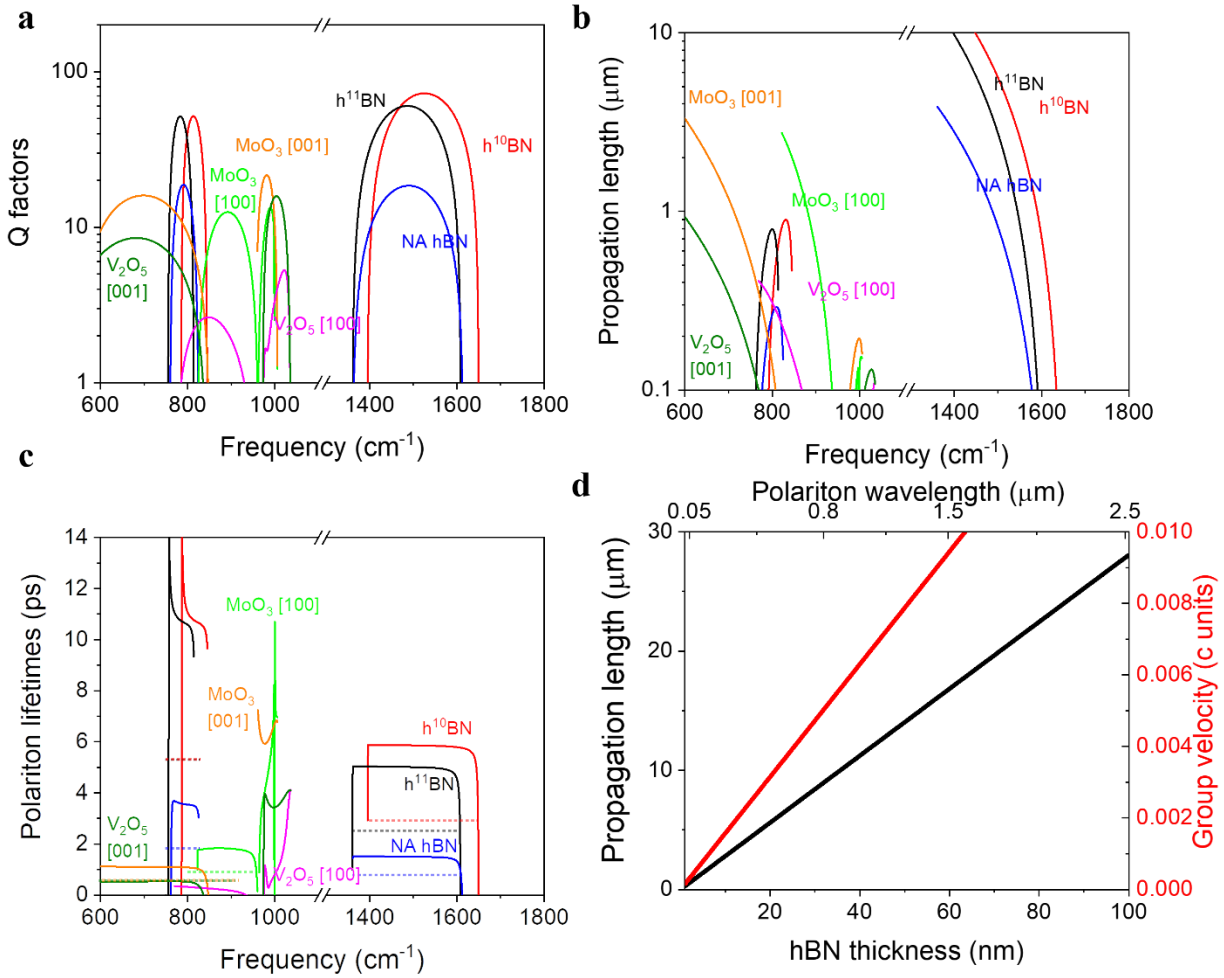

Fig. 10. Polariton Loss. (a) Q factors of HPhPs supported by different materials. (b) Propagation length of HPhPs supported by different materials. (c) Polariton lifetimes of HPhPs supported by different materials. Corresponding phonon lifetimes are plotted with dashed reference lines. Polariton lifetime is defined as $\tau = L_p/v_g$*, where* $v_g = \frac{\partial w}{\partial k}$ *is the group velocity. (d) Propagation length and group velocities of HPhPs supported by h^{10}BN. Note that the polariton lifetimes and Q-factors are irrelevant to hBN thicknesses.*

Opportunities in Polariton Anisotropy for Realizing Emergent Phenomena

Despite the above referenced advances, the community has still barely scratched the surface of the underlying physics and applications enabled by polariton anisotropy. Fruitful directions include identifying new materials, exploring nonlocal effects, and further advancements in twist-optics within heterogeneous structures. Below we highlight some specifics with reference to these directions.

Non-diagonalizable materials supporting low-loss polaritons: While significant gains can be made in realizing novel optical phenomena through artificial structuring of materials, it has arguably been through the identification of natural, highly anisotropic materials, where the most recent advances have been identified. Thus, it is reasonable to anticipate that further efforts in this regard will continue to be impactful. For instance, expanding the range of materials probed to lower symmetry crystals, including additional monoclinic and triclinic phases, for both SPhPs and SPPs is of immediate interest, building off the recent work in beta-phase Ga_2O_3.[18] Understanding the role that the off-diagonal elements of the permittivity tensor play in driving polariton losses and propagation can provide significant insights into what additional opportunities they can afford. Notably, several 2D materials offer such low symmetry crystal structures, while still maintaining the potential for exfoliating thin films, such as ReS_2, which is a triclinic, van der Waals crystal with low energy phonon modes[166] and the expectation of a series of broad bandwidth resonances in the far-infrared.

Nonlocal effects: As most of the phenomena involved in hybrid materials generally pushes the sizes of structures and layer thicknesses to levels approaching or below that of the fundamental excitations on which they are based (*e.g.*, electronic wavefunction, phonon wavelength), the role of non-local effects in driving emergent phenomena is of critical importance. Practically this results in changing optical properties as a function of confinement. While such nonlocal effects have been studied in plasmonic systems using cathodoluminescence,[167,168] s-SNOM,[169–172] EELS,[173,174], and polaritonic confinement[175] and theoretically explored using hydrodynamic models,[176–178] the impact of nonlocality in phononic systems has only recently started to be investigated.[23,162,163,179] Phononic nonlocality presents a unique phenomenology because, contrary to plasmonic systems that disperse towards the blue with reduced size, optic phonons have an anomalous dispersion causing them to shift towards the red at large wavevectors, leading to the possibility of resonant energy exchange and even strong coupling between transverse SPhPs and longitudinal phonons.[123,180,181] The resulting hybrid modes, called longitudinal-transverse phonon polaritons (LTPPs) were initially observed in 4H-SiC crystals[123] where the long unit cell along the c-axis folds the longitudinal optic phonon dispersion back into the light-line, giving rise to zone-

folded LO (ZFLO) phonons.[182] LTPP modes were then shown to be a general feature of nanostructures with nonlocal length scales and they were spectroscopically observed in crystalline hybrids.[179] As electrical currents in polar crystals lose energy primarily through the emission of LO phonons via the Fröhlich interaction, it has been theoretically predicted that LTPP modes can be used to alter electron-phonon interactions, resonantly coupling electrical currents to far-field radiation.[123] Although still in their infancy, the benefits of understanding nonlocality within phononic systems and hybrid structures promises to move beyond phenomena driven exclusively by the bulk permittivity tensors that are well described by effective medium approximations.

Twist-optics: Related to the creation of hybrid materials is the concept of twistronics. Manipulating the twist angle between the two layers of typically 2D material flakes enables the fine control of the electronic band structure (twistronics) – as well as new emergent optical properties.[144] For instance, materials such as bilayer graphene have been shown to display vastly different electronic behaviors from monolayer graphene,[140] ranging from non-conductive to superconductive conditions, with this conductivity sensitively dependent upon the angle between the principal crystal axes of the layers.[183] This concept has been applied to many other 2D materials, revealing exotic phenomena related to magnetism and transport. Note that the twist-optics we discuss here falls into two categories: structures where the properties are dictated by the electromagnetic hybrid (bulk property dictated) or atomic-stacking (atomic-level) methodologies. The former was discussed above, with the exemplary system of twisted layers of stacked MoO_3 and offers significant advantages. However, it is in the latter concept that the properties extend beyond those of the bulk permittivity tensors and emergent properties can be expected. For example, twisted graphene[183] system that can be used as a controllable circuit capable of routing plasmons with nanoscale precision by modifying the twist angle. Further, new collective excitations arising from interband electronic transitions in twisted bilayer graphene has been recently observed,[184,185] and others predicted, which includes chiral plasmons.[186] Other photonic phenomena, such as nonlinear responses such as second harmonic generation, have been demonstrated to be modulated and enhanced in twisted $MoSe_2/WS_2$.[187] Thus, even after extensive research efforts, the field of twist-optics is still relatively young and further theoretical and experimental studies are still required to provide insights into the emergence of optical topological transitions in 2D crystals, as well as the electromagnetic nature of the optical modes involved (note that the surface or volume character of canalized PhPs is still an open question). Further, extension of such twist-optics to incorporate materials of further reduced symmetries, such as exfoliated β-Ga_2O_3 flakes or ReS_2 will require further developments in our theoretical understanding, while promising opportunities to control the polaritonic properties more precisely.

Conclusions

Efforts such as those outlined above offer the potential to not only expand the current toolbox of available polaritonic materials, but more broadly to offer insights and understanding to unexplored emergent physics resulting from atomic-scale interactions and the nonlocal effects they induce. During the past two decades the materials and physical understandings of anisotropic polaritons have been evolving quickly, from artificial to natural, from isotropic to uniaxial, biaxial and more recently low symmetry and off-cut crystals, and the toolboxes to engineer such polaritons are expanding at a similarly fast rate. Despite those achievements, significant efforts are still necessary for this field, including physical understandings, material identifications, and fabrication techniques. The possibility of engineering materials with tailored optical response in the mid-infrared range opens up interesting perspectives for the use of these systems for optoelectronics.[188] The hybridization of longitudinal and transverse degrees of freedom due to nonlocal effects has already been theoretically predicted and experimentally observed in multiple systems.[22,123,162] We expect it will provide a channel for electrically-generated far-field emission of mid-infrared light without requiring complex injection minibands,[189] thus providing a simpler alternative to quantum cascade lasers. Thus, in concert, the combination of reduced crystal symmetry, hybrid polaritonic and phonon modes, nonlocal effects within near atomic scale systems and induced anisotropy through the field of twist-optics offer a collective path towards achieving novel optical and electro-optic devices where light can be generated, manipulated and directed with nanoscale precision.

Acknowledgements

M.H. and J.D.C. acknowledge support through the Army Research Office (Grant #W911NF-21-1-0119) and the National Science Foundation (Grant #1904793), respectively. T.G.F. acknowledges support through University of Iowa Startup funds and The Old Gold Fellowship. P.A.-G. and J.D. acknowledge support from the European Research Council under starting grant no. 715496, 2DNANOPTICA and the Spanish Ministry of Science and Innovation (State Plan for Scientific and Technical Research and Innovation grant number PID2019-111156GB-I00). S.D.L. acknowledges support by a Royal Society Research fellowship, the Philip Leverhulme prize, and a Research Grant of the Leverhulme Trust (Grant No. RPG-2019-174).

Funding sources

1. Army Research Office (Grant #W911NF-21-1-0119)
2. National Science Foundation (Grant #1904793)
3. University of Iowa Startup funds
4. The Old Gold Fellowship

5. The European Research Council under starting grant no. 715496
6. 2DNANOPTICA
7. Spanish Ministry of Science and Innovation (State Plan for Scientific and Technical Research and Innovation grant number PID2019-111156GB-I00)
8. Royal Society Research fellowship
9. Philip Leverhulme prize
10. Research Grant of the Leverhulme Trust (Grant No. RPG-2019-174)

REFERENCES

(1) Niu, S.; Joe, G.; Zhao, H.; Zhou, Y.; Orvis, T.; Huyan, H.; Salman, J.; Mahalingam, K.; Urwin, B.; Wu, J.; Liu, Y.; Tiwald, T. E.; Cronin, S. B.; Howe, B. M.; Mecklenburg, M.; Haiges, R.; Singh, D. J.; Wang, H.; Kats, M. A.; Ravichandran, J. Giant Optical Anisotropy in a Quasi-One-Dimensional Crystal. *Nat. Photonics* **2018**, *12*, 392–396.

(2) Caldwell, J. D.; Lindsay, L.; Giannini, V.; Vurgaftman, I.; Reinecke, T. L.; Maier, S. A.; Glembocki, O. J. Low-Loss, Infrared and Terahertz Nanophotonics Using Surface Phonon Polaritons. *Nanophotonics* **2015**, *4* (1), 44–68. https://doi.org/10.1515/nanoph-2014-0003.

(3) Basov, D. N.; Fogler, M. M.; García De Abajo, F. J. Polaritons in van Der Waals Materials. *Science (80-.).* **2016**, *354* (6309), aag1992. https://doi.org/10.1126/science.aag1992.

(4) Low, T.; Chaves, A.; Caldwell, J. D.; Kumar, A.; Fang, N. X.; Avouris, P.; Heinz, T. F.; Guinea, F.; Martin-Moreno, L.; Koppens, F. Polaritons in Layered Two-Dimensional Materials. *Nat. Mater.* **2017**, *16*, 182–194. https://doi.org/10.1038/nmat4792.

(5) Foteinopoulou, S.; Devarapu, G. C. R.; Subramania, G. S.; Krishna, S.; Wasserman, D. Phonon-Polaritonics: Enabling Powerful Capabilities for Infrared Photonics. *Nanophotonics* **2019**, *8* (12), 2129–2175. https://doi.org/10.1515/nanoph-2019-0232.

(6) Poddubny, A.; Iorsh, I.; Belov, P.; Kivshar, Y. Hyperbolic Metamaterials. *Nat. Photonics* **2013**, *7* (12), 948–957. https://doi.org/10.1038/nphoton.2013.243.

(7) Ma, W.; Shabbir, B.; Ou, Q.; Dong, Y.; Chen, H.; Li, P.; Zhang, X. Anisotropic Polaritons in van Der Waals Materials. *InfoMat* **2020**, *2* (5), 777–790.

(8) Caldwell, J. D.; Kretinin, A. V.; Chen, Y.; Giannini, V.; Fogler, M. M.; Francescato, Y.; Ellis, C. T.; Tischler, J. G.; Woods, C. R.; Giles, A. J.; Hong, M.; Watanabe, K.; Taniguchi, T.; Maier, S. A.; Novoselov, K. S. Sub-Diffractional Volume-Confined Polaritons in the Natural Hyperbolic Material Hexagonal Boron Nitride. *Nat. Commun.* **2014**, *5*. https://doi.org/10.1038/ncomms6221.

(9) Dai, S.; Fei, Z.; Ma, Q.; Rodin, A. S.; Wagner, M.; McLeod, A. S.; Liu, M. K.; Gannett, W.; Regan, W.; Thiemens, M.; Dominguez, G.; Castro Neto, A. H.; Zettl, A.; Keilmann, F.; Jarillo-Herrero, P.; Fogler, M. M.; Basov, D. N. Tunable Phonon Polaritons in Atomically Thin van Der Waals Crystals of Boron Nitride. *Science (80-.).* **2014**, *343* (6175), 1125–1129.

(10) Estevam da Silva, R.; Macedo, R.; Dumelow, T.; da Costa, J. A. P.; Honorato, S. B.; Ayala, A. P. Far-Infrared Slab Lensing and Subwavelength Imaging in Crystal Quartz. *Phys. Rev. B* **2012**, *86*, 155152.

(11) Korzeb, K.; Gajc, M.; Pawlak, D. A. Compendium of Natural Hyperbolic Materials. *Opt. Express* **2015**, *23* (20), 25406–25424.

(12) Narimanov, E. E.; Kildishev, A. V. Naturally Hyperbolic. *Nat. Photonics* **2015**, *9*, 214–216.

(13) Li, P.; Dolado, I.; Alfaro-Mozaz, F. J.; Casanova, F.; Hueso, L. E.; Liu, S.; Edgar, J. H.; Nikitin, A. Y.; Vélez, S.; Hillenbrand, R.; Javier Alfaro-Mozaz, F.; Casanova, F.; Hueso, L. E.; Liu, S.; Edgar, J. H.; Nikitin, A. Y.; Velez, S.; Hillenbrand, R. Infrared Hyperbolic Metasurface Based on Nanostructured van Der Waals Materials. *Science (80-.).* **2018**, *359* (6378), 892–896. https://doi.org/10.1126/science.aaq1704.

(14) Ma, W.; Alonso-González, P.; Li, S.; Nikitin, A. Y.; Yuan, J.; Martín-Sánchez, J.; Taboada-Gutiérrez, J.; Amenabar, I.; Li, P.; Vélez, S.; Tollan, C.; Dai, Z.; Zhang, Y.; Sriram, S.; Kalantar-Zadeh, K.; Lee, S. T.; Hillenbrand, R.; Bao, Q. In-Plane Anisotropic and Ultra-Low-Loss Polaritons in a Natural van Der Waals Crystal. *Nature* **2018**, *562*, 557–562. https://doi.org/10.1038/s41586-018-0618-9.

(15) Zheng, Z.; Xu, N.; Oscurato, S. L.; Tamagnone, M.; Sun, F.; Jiang, Y.; Ke, Y.; Chen, J.; Huang, W.; Wilson, W. L.; Ambrosio, A.; Deng, S.; Chen, H. A Mid-Infrared Biaxial Hyperbolic van Der Waals Crystal. *Sci. Adv.* **2019**, *5* (5), eaav8690. https://doi.org/10.1126/sciadv.aav8690.

(16) Taboada-Gutiérrez, J.; Álvarez-Pérez, G.; Duan, J.; Ma, W.; Crowley, K.; Prieto, I.; Bylinkin, A.; Autore, M.; Volkova, H.; Kimura, K.; Kimura, T.; Berger, M. H.; Li, S.; Bao, Q.; Gao, X. P. A.; Errea, I.; Nikitin, A. Y.; Hillenbrand, R.; Martín-Sánchez, J.; Alonso-González, P. Broad Spectral Tuning of

Ultra-Low-Loss Polaritons in a van Der Waals Crystal by Intercalation. *Nat. Mater.* **2020**, *19*, 964–868. https://doi.org/10.1038/s41563-020-0665-0.

(17) Ma, W.; Hu, G.; Hu, D.; Chen, R.; Sun, T.; Zhang, X.; Dai, Q.; Zeng, Y.; Alu, A.; Qiu, C.-W.; Li, P. Ghost Hyperbolic Surface Polaritons in Bulk Anisotropic Crystals. *Nature* **2021**, *596*, 362–366.

(18) Passler, N. C.; Ni, X.; Hu, G.; Matson, J. R.; Wolf, M.; Schubert, M.; Alu, A.; Caldwell, J. D.; Folland, T. G.; Paarmann, A. Hyperbolic Shear Polaritons in Low-Symmetry Crystals. *Nature* **2022**, 602, 595–600. https://doi.org/10.1038/s41586-021-04328-y*under revi*.

(19) Dai, S.; Ma, Q.; Liu, M. K.; Anderson, T.; Fei, Z.; Goldflam, M. D.; Wagner, M.; Watanabe, K.; Taniguchi, T.; Thiemens, M.; Keilmann, F.; Janssen, G. C. A. M.; Zhu, S.-E.; Jarillo-Herrero, P.; Fogler, M. M.; Basov, D. N. Graphene on Hexagonal Boron Nitride as a Tunable Hyperbolic Metamaterial. *Nat. Nanotechnol.* **2015**, *10*, 682–686.

(20) Caldwell, J. D.; Novoselov, K. S. Mid-Infrared Nanophotonics. *Nat. Mater.* **2015**, *14*, 364–365.

(21) Caldwell, J. D.; Vurgaftman, I.; Tischler, J. G.; Glembocki, O. J.; Owrutsky, J. C.; Reinecke, T. L. Atomic-Scale Photonic Hybrids for Mid-Infrared and Terahertz Nanophotonics. *Nature Nanotechnology*. 2016. https://doi.org/10.1038/nnano.2015.305.

(22) Ratchford, D. C.; Winta, C. J.; Chatzakis, I.; Ellis, C. T.; Passler, N. C.; Winterstein, J.; Dev, P.; Razdolski, I.; Matson, J. R.; Nolen, J. R.; Tischler, J. G.; Vurgaftman, I.; Katz, M. B.; Nepal, N.; Hardy, M. T.; Hachtel, J. A.; Idrobo, J. C.; Reinecke, T. L.; Giles, A. J.; Katzer, D. S.; Bassim, N. D.; Stroud, R. M.; Wolf, M.; Paarmann, A.; Caldwell, J. D. Controlling the Infrared Dielectric Function through Atomic-Scale Heterostructures. *ACS Nano* **2019**, *13* (6), 6730–6741. https://doi.org/10.1021/acsnano.9b01275.

(23) Gubbin, C. R.; De Liberato, S. Optical Nonlocality in Polar Dielectrics. *Phys. Rev. X* **2020**, *10*, 021027.

(24) Duan, J.; Capote-Robayna, N.; Taboada-Gutiérrez, J.; Álvarez-Pérez, G.; Prieto, I.; Martín-Sánchez, J.; Nikitin, A. Y.; Alonso-González, P. Twisted Nano-Optics: Manipulating Light at the Nanoscale with Twisted Phonon Polaritonic Slabs. *Nano Lett.* **2020**. https://doi.org/10.1021/acs.nanolett.0c01673.

(25) Sheinfux, H. H.; Koppens, F. H. L. The Rise of Twist-Optics. *Nano Lett.* **2020**, *20* (10), 6935–6936.

(26) Joulain, K.; Carminati, R.; Mulet, J.-P.; Greffet, J.-J. Definition and Measurement of the Local Density of Electromagnetic States Close to an Interface. *Phys. Rev. B* **2003**, *68*, 245405.

(27) Neuman, T.; Alonso-González, P.; Garcia-Etxarri, A.; Schnell, M.; Hillenbrand, R.; Aizpurua, J. Mapping the near Fields of Plasmonic Nanoantennas by Scattering-Type Scanning near-Field Optical Microscopy. *Laser Photon. Rev.* **2015**, *9* (6), 637–649.

(28) Barnes, W. L.; Horsley, S. A. R.; Vos, W. L. Classical Antennas, Quantum Emitters, and Densities of Optical States. *J. Opt.* **2020**, *22*, 073501.

(29) Chen, X.; Hu, D.; Mescall, R.; You, G.; Basov, D. N.; Dai, Q.; Liu, M. Modern Scattering-Type Scanning Near-Field Optical Microscopy for Advanced Material Research. *Adv. Mater.* **2019**, *31* (24), 1804774.

(30) Folland, T. G.; Nordin, L.; Wasserman, D.; Caldwell, J. D. Probing Polaritons in the Mid- to Far-Infrared. *J. Appl. Phys.* **2019**, *125* (19), 191102. https://doi.org/10.1063/1.5090777.

(31) Dai, S.; Ma, Q.; Yang, Y.; Rosenfeld, J.; Goldflam, M. D.; McLeod, A. S.; Sun, Z.; Andersen, T. I.; Fei, Z.; Liu, M.; Shao, Y.; Watanabe, K.; Taniguchi, K.; Thiemens, M.; Keilmann, F.; Jarillo-Herrero, P.; Fogler, M. M.; Basov, D. N.; Taniguchi, T.; Thiemens, M.; Keilmann, F.; Jarillo-Herrero, P.; Fogler, M. M.; Basov, D. N. Efficiency of Launching Highly Confined Polaritons by Infrared Light Incident on a Hyperbolic Material. *Nano Lett.* **2017**, *17* (9), 5285–5290. https://doi.org/10.1021/acs.nanolett.7b01587.

(32) Pons-Valencia, P.; Alfaro-Mozaz, F. J.; Wiecha, M. M.; Biolek, V.; Dolado, I.; Vélez, S.; Li, P.; Alonso-González, P.; Casanova, F.; Hueso, L. E.; Martín-Moreno, L.; Hillenbrand, R.; Nikitin, A. Y. Launching of Hyperbolic Phonon-Polaritons in h-BN Slabs by Resonant Metal Plasmonic Antennas. *Nat. Commun.* **2019**, *10* (1), 1–8. https://doi.org/10.1038/s41467-019-11143-7.

(33) Wang, T.; Li, P.; Chigrin, D. N.; Giles, A. J.; Bezares, F. J.; Glembocki, O. J.; Caldwell, J. D.; Taubner, T. Phonon-Polaritonic Bowtie Nanoantennas: Controlling Infrared Thermal Radiation at the Nanoscale. *ACS Photonics* **2017**, *4* (7), 1753–1760. https://doi.org/10.1021/acsphotonics.7b00321.

(34) P., A.-G.; Y., N. A.; F., G.; A., C.; A., P.; S., V.; J., C.; G., N.; F., K.; A., Z.; F., C.; E., H. L.; R., H. Controlling Graphene Plasmons with Resonant Metal Antennas and Spatial Conductivity Patterns. *Science (80-.).* **2014**, *344* (6190), 1369–1373. https://doi.org/10.1126/science.1253202.

(35) Giles, A. J.; Dai, S.; Glembocki, O. J.; Kretinin, A. V.; Sun, Z.; Ellis, C. T.; Tischler, J. G.; Taniguchi, T.; Watanabe, K.; Fogler, M. M.; Novoselov, K. S.; Basov, D. N.; Caldwell, J. D. Imaging of Anomalous Internal Reflections of Hyperbolic Phonon-Polaritons in Hexagonal Boron Nitride. *Nano Lett.* **2016**, *16* (6), 3858–3865. https://doi.org/10.1021/acs.nanolett.6b01341.

(36) Dereshgi, S. A.; Folland, T. G.; Murthy, A. A.; Song, X.; Tanriover, I.; Dravid, V. P.; Caldwell, J. D.; Aydin, K. Lithography-free IR polarization converters via orthogonal in-plane phonons in α-MoO3 flakes. Nat. Commun. **2020**, 11, 5771. https://doi.org/10.1038/s41467-020-19499-x

(37) Ramer, G.; Tuteja, M.; Matson, J. R.; Davanco, M.; Folland, T. G.; Kretinin, A.; Taniguchi, T.; Watanabe, K.; Novoselov, K. S.; Caldwell, J. D.; Centrone, A. High-Q Dark Hyperbolic Phonon-Polaritons in Hexagonal Boron Nitride Nanostructures. *Nanophotonics* **2020**, *9* (6), 1457–1467. https://doi.org/10.1515/nanoph-2020-0048.

(38) Tamagnone, M.; Ambrosio, A.; Chaudhary, K.; Jauregui, L. A.; Kim, P.; Wilson, W. L.; Capasso, F. Ultra-Confined Mid-Infrared Resonant Phonon Polaritons in van Der Waals Nanostructures. *Sci. Adv.* **2018**, *6* (4), eaat7189.

(39) Xu, X. G.; Ghamsari, B. G.; Jiang, J.-H.; Gilburd, L.; Andreev, G. O.; Zhi, C.; Bando, Y.; Golberg, D.; Berini, P.; Walker, G. C. One-Dimensional Surface Phonon Polaritons in Boron Nitride Nanotubes. *Nat. Commun.* **2014**, *5* (1), 4782. https://doi.org/10.1038/ncomms5782.

(40) Sohr, P.; Law, S. Structural Parameters of Hyperbolic Metamaterials Controlling High-k Mode Resonant Wavelengths. *J. Opt. Soc. Am. B* **2020**, *37* (12), 3784–3791.

(41) Sohr, P.; Wei, D.; Wang, Z.; Law, S. Strong Coupling in Semiconductor Hyperbolic Metamaterials. *Nano Lett.* **2021**, *21* (23), 9951–9957.

(42) Folland, T. G.; Lu, G.; Bruncz, A.; Nolen, J. R.; Tadjer, M.; Caldwell, J. D. Vibrational Coupling to Epsilon-Near-Zero Waveguide Modes. *ACS Photonics* **2020**, *7* (3), 614–621. https://doi.org/10.1021/acsphotonics.0c00071.

(43) Greffet, J.-J.; Carminati, R.; Joulain, K.; Mulet, J. P.; Mainguy, S. P.; Chen, Y. Coherent Emission of Light by Thermal Sources. *Nature* **2002**, *416* (6876), 61–64.

(44) Folland, T. G.; Ma, T. W. W.; Matson, J. R.; Nolen, J. R.; Liu, S.; Watanabe, K.; Taniguchi, T.; Edgar, J. H.; Taubner, T.; Caldwell, J. D. Probing Hyperbolic Polaritons Using Infrared Attenuated Total

Reflectance Micro-Spectroscopy. *MRS Commun.* **2018**, *8* (4), 1418–1425. https://doi.org/10.1557/mrc.2018.205.

(45) Passler, N. C.; Gubbin, C. R.; Folland, T. G.; Razdolski, I.; Katzer, D. S.; Storm, D. F.; Wolf, M.; De Liberato, S.; Caldwell, J. D.; Paarmann, A. Strong Coupling of Epsilon-Near-Zero Phonon Polaritons in Polar Dielectric Heterostructures. *Nano Lett.* **2018**, *18* (7), 4285–4292. https://doi.org/10.1021/acs.nanolett.8b01273.

(46) Runnerstrom, E. L.; Kelley, K. P.; Sachet, E.; Shelton, C. T.; Maria, J. P. Epsilon-near-Zero Modes and Surface Plasmon Resonance in Fluorine-Doped Cadmium Oxide Tin Films. *ACS Photonics* **2017**, *4* (8), 1885–1892.

(47) Passler, N. C.; Razdolski, I.; Katzer, D. S.; Storm, D. F.; Caldwell, J. D.; Wolf, M.; Paarmann, A. Second Harmonic Generation from Phononic Epsilon-Near-Zero Berreman Modes in Ultrathin Polar Crystal Films. *ACS Photonics* **2019**, *6* (6). https://doi.org/10.1021/acsphotonics.9b00290.

(48) He, Mingze, J. Ryan Nolen, Josh Nordlander, Angela Cleri, Nathaniel S. McIlwaine, Yucheng Tang, Guanyu Lu et al. "Deterministic inverse design of Tamm plasmon thermal emitters with multi-resonant control." Nature Materials **2021**, 12, 1663-1669.

(49) Alfaro-Mozaz, F. J.; Rodrigo, S. G.; Alonso-González, P.; Velez, S.; Casanova, F.; Hueso, L. E.; Martin-Moreno, L.; Hillenbrand, R.; Nikitin, A. Y. Deeply Subwavelength Phonon-Polaritonic Crystal Made of a van Der Waals Material. *Nat. Commun.* **2019**, *10*, 42.

(50) Alfaro-Mozaz, F. J.; Rodrigo, S. G.; Vélez, S.; Dolado, I.; Govyadinov, A.; Alonso-González, P.; Casanova, F.; Hueso, L. E.; Martín-Moreno, L.; Hillenbrand, R.; Nikitin, A. Y. Hyperspectral Nanoimaging of van Der Waals Polaritonic Crystals. *Nano Lett.* **2021**, *21* (17), 7109–7115. https://doi.org/10.1021/acs.nanolett.1c01452.

(51) Yang, J.; Krix, Z. E.; Kim, S.; Tang, J.; Mayyas, M.; Wang, Y.; Watanabe, K.; Taniguchi, T.; Li, L. H.; Hamilton, A. R.; Aharonovich, I.; Sushkov, O. P.; Kalantar-Zadeh, K. Near-Field Excited Archimedean-like Tiling Patterns in Phonon-Polaritonic Crystals. *ACS Nano* **2021**, *15* (5), 9134–9142. https://doi.org/10.1021/acsnano.1c02507.

(52) Guddala, S.; Komissarenko, F.; Kiriushechkina, S.; Vakulenko, A.; Li, M.; Menon, V. M.; Alù, A.; Khanikaev, A. B. Topological Phonon-Polariton Funneling in Midinfrared Metasurfaces. *Science (80-.).* **2021**, *374* (6564), 225–227. https://doi.org/10.1126/science.abj5488.

(53) Kim, S.; Fröch, J. E.; Christian, J.; Straw, M.; Bishop, J.; Totonjian, D.; Watanabe, K.; Taniguchi, T.; Toth, M.; Aharonovich, I. Photonic Crystal Cavities from Hexagonal Boron Nitride. *Nat. Commun.* **2018**, *9* (1), 2623. https://doi.org/10.1038/s41467-018-05117-4.

(54) Adachi, S. The Reststrahlen Region. In *Optical Properties of Crystalline and Amorphous Semiconductors: Materials and Fundamental Principles*; Springer Science+Business Media, LLC: New York, NY, 1999; pp 33–61.

(55) Maier, S. A. *Plasmonics: Fundamentals and Applications*; Springer-Verlag US: Berlin, 2007.

(56) Basov, D. N.; Asenjo-Garcia, A.; Schuck, P. J.; Zhu, X.; Rubio, A. Polariton Panorama. *Nanophotonics* **2021**, *10* (1), 549–577. https://doi.org/doi:10.1515/nanoph-2020-0449.

(57) Kavokin, A.; Baumberg, J. J.; Malpuech, G.; Laussy, F. P. *Microcavities*; Oxford University Press: New York, NY, 2011.

(58) Hu, F.; Fei, Z. Recent Progress on Exciton Polaritons in Layered Transition-Metal Dichalcogenides. *Adv. Opt. Mater.* **2020**, *8* (5), 1901003.

(59) Curtis, J. B.; Grankin, A.; Poniatowski, N. R.; etc. Cavity magnon-polaritons in cuprate parent compounds. Submitted on 15 Jun 2021. ArXiv.org, cond-mat, arXiv:2106.07828v1 (accessed 2022-02-10).

(60) Juraschek, D. M.; Wang, D. S.; Narang, P. Sum-Frequency Excitation of Coherent Magnons. *Phys. Rev. B* **2021**, *103*, 094407.

(61) Ballarini, D.; De Liberato, S. Polaritonics: From Microcavities to Sub-Wavelength Confinement. *Nanophotonics* **2019**, *8* (4), 641–654.

(62) Bayer, A.; Pozimski, M.; Schambeck, S.; Schuh, D.; Huber, R.; Bougeard, D.; Lange, C. Terahertz Light–Matter Interaction beyond Unity Coupling Strength. *Nano Lett.* **2017**, *17* (10), 6340–6344. https://doi.org/10.1021/acs.nanolett.7b03103.

(63) Li, X.; Bamba, M.; Zhang, Q.; Fallahi, S.; Gardner, G. C.; Gao, W.; Lou, M.; Yoshioka, K.; Manfra, M. J.; Kono, J. Vacuum Bloch–Siegert Shift in Landau Polaritons with Ultra-High Cooperativity. *Nat. Photonics* **2018**, *12* (6), 324–329. https://doi.org/10.1038/s41566-018-0153-0.

(64) G., S.; C., M.; D., T.; D., H.; S., D. L.; C., C.; C., R.; D., S.; W., W.; M., B.; J., F. Ultrastrong Coupling of the Cyclotron Transition of a 2D Electron Gas to a THz Metamaterial. *Science (80-.).* **2012**, *335*

(6074), 1323–1326. https://doi.org/10.1126/science.1216022.

(65) Xiang, B.; Ribeiro, R. F.; Dunkelberger, A. D.; Wang, J.; Li, Y.; Simpkins, B. S.; Owrutsky, J. C.; Yuen-Zhou, J.; Xiong, W. Two-Dimensional Infrared Spectroscopy of Vibrational Polaritons. *Proc. Natl. Acad. Sci.* **2018**, *115* (19), 4845–4850. https://doi.org/10.1073/pnas.1722063115.

(66) Simpkins, B. S.; Fears, K. P.; Dressick, W. J.; Spann, B. T.; Dunkelberger, A. D.; Owrutsky, J. C. Spanning Strong to Weak Normal Mode Coupling between Vibrational and Fabry-Perot Cavity Modes through Tuning of Vibrational Absorption Strength. *ACS Photonics* **2015**, *2* (10), 1460–1467. https://doi.org/10.1021/acsphotonics.5b00324.

(67) Hutchison, J. A.; Schwartz, T.; Genet, C.; Devaux, E.; Ebbesen, T. W. Modifying Chemical Landscapes by Coupling to Vacuum Fields. *Angew. Chemie - Int. Ed.* **2012**, *51* (7), 1592–1596. https://doi.org/10.1002/anie.201107033.

(68) Juraschek, D. M.; Neuman, T.; Flick, J.; Narang, P. Cavity Control of Nonlinear Phononics. *Phys. Rev. Res.* **2021**, *3*, L032046.

(69) Rivera, N.; Flick, J.; Narang, P. Variational Theory of Nonrelativistic Quantum Electrodynamics. *Phys. Rev. Lett.* **2019**, *122*, 192603.

(70) Long, J. P.; Simpkins, B. S. Coherent Coupling between a Molecular Vibration and Fabry–Perot Optical Cavity to Give Hybridized States in the Strong Coupling Limit. *ACS Photonics* **2015**, *2* (1), 130–136. https://doi.org/10.1021/ph5003347.

(71) Shalabney, A.; George, J.; Hutchinson, J.; Pupillo, G.; Genet, C.; Ebbesen, T. W. Coherent Coupling of Molecular Resonators with a Microcavity Mode. *Nat. Commun.* **2015**, *6*, 5981.

(72) Caldwell, J. D.; Aharonovich, I.; Cassabois, G.; Edgar, J. H.; Gil, B.; Basov, D. N. Photonics with Hexagonal Boron Nitride. *Nat. Rev. Mater.* **2019**, *4* (8), 552–567. https://doi.org/10.1038/s41578-019-0124-1.

(73) Born, M.; Wolf, E. *Principles of Optics, 60th Anniversary Edition*, 7th Editio.; Cambridge University Press: Cambridge, UK, 2020.

(74) Álvarez-Pérez, G.; Voronin, K. V; Volkov, V. S.; Alonso-González, P.; Nikitin, A. Y. Analytical Approximations for the Dispersion of Electromagnetic Modes in Slabs of Biaxial Crystals. *Phys. Rev. B* **2019**, *100* (23), 235408. https://doi.org/10.1103/PhysRevB.100.235408.

(75) Giles, A. J.; Dai, S.; Glembocki, O. J.; Kretinin, A. V.; Sun, Z.; Ellis, C. T.; Tischler, J. G.; Taniguchi, T.; Watanabe, K.; Fogler, M. M.; Novoselov, K. S.; Basov, D. N.; Caldwell, J. D. Imaging of Anomalous Internal Reflections of Hyperbolic Phonon-Polaritons in Hexagonal Boron Nitride. *Nano Lett.* **2016**, *16* (6), 3858–3865. https://doi.org/10.1021/acs.nanolett.6b01341.

(76) Breslin, V. M.; Ratchford, D. C.; Giles, A. J.; Dunkelberger, A. D.; Owrutsky, J. C. Hyperbolic Phonon Polariton Resonances in Calcite Nanopillars. *Opt. Express* **2021**, *29* (8), 11760–11772. https://doi.org/10.1364/OE.417405.

(77) Sun, J.; Litchinitser, N. M.; Zhou, J. Indefinite by Nature: From Ultraviolet to Terahertz. *ACS Photonics* **2014**, *1* (4), 293–303.

(78) Jacob, Z.; Kim, J.-Y.; Naik, G. V; Boltasseva, A.; Narimanov, E. E.; Shalaev, V. M. Engineering Photonic Density of States Using Metamaterials. *Appl. Phys. B* **2010**, *100* (1), 215–218.

(79) Folland, T. G.; Caldwell, J. D. Precise Control of Infrared Polarization Using Crystal Vibrations. *Nature* **2018**, *562*, 499–501. https://doi.org/10.1038/d41586-018-07087-5.

(80) Caldwell, J. D. Caldwell Nanophotonic Materials and Devices Lab. URL: https://my.vanderbilt.edu/caldwellgroup/. (acessed 2022-Feb-03)

(81) Zheng, Z.; Chen, J.; Wang, Y.; Wang, X.; Chen, X.; Liu, P.; Xu, J.; Xie, W.; Chen, H.; Deng, S.; Xu, N. Highly Confined and Tunable Hyperbolic Phonon Polaritons in Van Der Waals Semiconducting Transition Metal Oxides. *Adv. Mater.* **2018**, *30* (13), 1705318. https://doi.org/10.1002/adma.201705318.

(82) Álvarez-Pérez, G.; Folland, T. G.; Errea, I.; Taboada-Gutiérrez, J.; Duan, J.; Martín-Sánchez, J.; Tresguerres-Mata, A. I. F.; Matson, J. R.; Bylinkin, A.; He, M.; Ma, W.; Bao, Q.; Martín, J. I.; Caldwell, J. D.; Nikitin, A. Y.; Alonso-González, P. Infrared Permittivity of the Biaxial van Der Waals Semiconductor α-MoO3 from Near- and Far-Field Correlative Studies. *Adv. Mater.* **2020**, *32* (29), 1908176. https://doi.org/10.1002/adma.201908176.

(83) Caldwell, J. D.; Stahlbush, R. E.; Mahadik, N. A. Mitigating Defects within Silicon Carbide Epitaxy. In *ECS Transactions*; 2011; Vol. 41. https://doi.org/10.1149/1.3631503.

(84) Drachev, V. P.; Podolskiy, V. A.; Kildishev, A. V. Hyperbolic Metamaterials: New Physics behind a Classical Problem. *Opt. Express* **2013**, *21* (12), 15048–15064.

(85) Shekhar, P.; Atkinson, J.; Jacob, Z. Hyperbolic Metamaterials: Fundamentals and Applications. *Nano Converg.* **2014**, *1*, 14.

(86) Smith, D. R.; Vier, D. C.; Koschny, T.; Soukoulis, C. M. Electromagnetic Parameter Retrieval from Inhomogeneous Metamaterials. *Phys. Rev. E Stat. Physics, Plasmas, Fluids, Relat. Interdiscip. Top.* **71AD**, No. 036617.

(87) Hoffman, A. J.; Alekseyev, L.; Howard, S. S.; Franz, K. J.; Wasserman, D.; Podolskiy, V. A.; Narimanov, E. E.; Sivco, D. L.; Gmachl, C. Negative Refraction in Semiconductor Metamaterials. *Nat. Mater.* **2007**, *6* (12), 946–950.

(88) Korobkin, D.; Neuner, B.; Fietz, C.; Jegenyes, N.; Ferro, G.; Shvets, G. Measurements of the Negative Refractive Index of Sub-Diffraction Waves Propagating in an Indefinite Permittivity Medium. *Opt. Express* **2010**, *18* (22), 22734–22746.

(89) Smith, D. R.; Pendry, J. B.; Wiltshire, M. C. Metamaterials and Negative Refractive Index. *Sci.* **2004**, *305*, 788–792.

(90) Kullock, R.; Grafstrom, S.; Evans, P. R.; Pollard, R. J.; Eng, L. M. Metallic Nanorod Arrays: Negative Refraction and Optical Properties Explained by Retarded Dipolar Interactions. *J. Opt. Soc. Am. B Opt. Phys.* **2001**, *27* (9), 1819–1827.

(91) Pendry, J. B. Negative Refraction Makes a Perfect Lens. *Phys. Rev. Lett.* **2000**, *85* (18), 3966–3969.

(92) Shalaev, V. M.; Cai, W.; Chettiar, U. K.; Yuan, H.-K.; Sarychev, A. K.; Drachev, V. P.; Kildishev, A. V. Negative Index of Refraction in Optical Metamaterials. *Opt. Lett.* **2005**, *30* (24), 3356–3358.

(93) Jacob, Z.; Alekseyev, L. V.; Narimanov, E. Optical Hyperlens: Far-Field Imaging Beyond the Diffraction Limit. *Opt. Express* **2006**, *14* (18), 8247–8256.

(94) Liu, Z.; Lee, H.; Xiong, Y.; Sun, C.; Zhang, X. Far-Field Optical Hyperlens Magnifying Sub-Diffraction-Limited Objects. *Sci.* **2007**, *315*, 1686-.

(95) Salandrino, A.; Engheta, N. Far-Field Subdiffraction Optical Microscopy Using Metamaterial Crystals: Theory and Simulations. *Phys. Rev. B* **2006**, *74*, 75103.

(96) Li, P.; Lewin, M.; Kretinin, A. V.; Caldwell, J. D.; Novoselov, K. S.; Taniguchi, T.; Watanabe, K.; Gaussmann, F.; Taubner, T. Hyperbolic Phonon-Polaritons in Boron Nitride for near-Field Optical Imaging and Focusing. *Nat. Commun.* **2015**, *6*, 7507. https://doi.org/10.1038/ncomms8507.

(97) Dai, S.; Ma, Q.; Anderson, T.; McLeod, A. S.; Fei, Z.; Liu, M. K.; Wagner, M.; Watanabe, K.; Taniguchi, T.; Thiemens, M.; Keilmann, F.; Jarillo-Herrero, P.; Fogler, M. M.; Basov, D. N. Subdiffractional Focusing and Guiding of Polaritonic Rays in a Natural Hyperbolic Material. *Nat. Commun.* **2015**, *6*, 6963.

(98) Sun, J.; Litchinitser, N. M. Toward Practical, Subwavelength, Visible-Light Photolithography with Hyperlens. *ACS Nano* **2018**, *12* (1), 542–548.

(99) Xiong, Y.; Liu, Z.; Zhang, X. A Simple Design of Flat Hyperlens for Lithography and Imaging with Half-Pitch Resolution down to 20 Nm. *Appl. Phys. Lett.* **2009**, *94* (20), 203108.

(100) Khurgin, J. B.; Boltasseva, A. Reflecting upon the Losses in Plasmonics and Metamaterials. *MRS Bull.* **2012**, *37*, 768–779.

(101) Khurgin, J. B.; Sun, G. Scaling of Losses with Size and Wavelength in Nanoplasmonics and Metamaterials. *Appl. Phys. Lett.* **2011**, *99*, 211106.

(102) Boltasseva, A.; Atwater, H. A. Low-Loss Plasmonic Metamaterials. *Sci.* **2011**, *331* (6015), 290–291.

(103) Giles, A. J.; Dai, S.; Vurgaftman, I.; Hoffman, T.; Liu, S.; Lindsay, L.; Ellis, C. T.; Assefa, N.; Chatzakis, I.; Reinecke, T. L.; Tischler, J. G.; Fogler, M. M.; Edgar, J. H.; Basov, D. N.; Caldwell, J. D. Ultra-Low-Loss Polaritons in Isotopically Pure Boron Nitride. *Nat. Mater.* **2018**, *17* (2), 134–139. https://doi.org/10.1038/NMAT5047.

(104) Dai, S.; Fang, W.; Rivera, N.; Stehle, Y.; Jiang, B.-Y.; Shen, J.; Tay, R. Y.; Ciccarino, C. J.; Ma, Q.; Rodan-Legrain, D.; Jarillo-Herrero, P.; Teo, E. H. T.; Fogler, M. M.; Narang, P.; Kong, J.; Basov, D. N. Phonon Polaritons in Monolayers of Hexagonal Boron Nitride. *Adv. Mater.* **2019**, *31* (37), 1806603. https://doi.org/https://doi.org/10.1002/adma.201806603.

(105) Rivera, N.; Christensen, T.; Narang, P. Phonon Polaritonics in Two-Dimensional Materials. *Nano Lett.* **2019**, *19* (4), 2653–2660. https://doi.org/10.1021/acs.nanolett.9b00518.

(106) Li, N.; Guo, X.; Yang, X.; Qi, R.; Qiao, T.; Li, Y.; Shi, R.; Li, Y.; Liu, K.; Xu, Z.; Liu, L.; García de Abajo, F. J.; Dai, Q.; Wang, E.-G.; Gao, P. Direct Observation of Highly Confined Phonon Polaritons in Suspended Monolayer Hexagonal Boron Nitride. *Nat. Mater.* **2021**, *20* (1), 43–48. https://doi.org/10.1038/s41563-020-0763-z.

(107) He, M.; Iyer, G. R. S.; Aarav, S.; Sunku, S. S.; Giles, A. J.; Folland, T. G.; Sharac, N.; Sun, X.; Matson,

J. R.; Liu, S.; Edgar, J. H.; Fleischer, J. W.; Basov, D. N.; Caldwell, J. D. Ultrahigh-Resolution, Label-Free Hyperlens Imaging in the Mid-IR. *Nano Lett.* **2021**, 21(19), 7921–7928. DOI: *10.1021/acs.nanolett.1c01808*

(108) Lee, I.-H.; He, M.; Zhang, X.; Luo, Y.; Liu, S.; Edgar, J. H.; Wang, K.; Avouris, P.; Low, T.; Caldwell, J. D.; Oh, S.-H. Image Polaritons in Boron Nitride for Extreme Polariton Confinement with Low Losses. *Nat. Commun.* **2020**, *11*, 3649. https://doi.org/10.1038/s41467-020-17424-w.

(109) Yoxall, E.; Schnell, M.; Nikitin, A. Y.; Txoperena, O.; Woessner, A.; Lundeberg, M. B.; Casanova, F.; Hueso, L. E.; Koppens, F. H. L.; Hillenbrand, R. Direct Observation of Ultraslow Hyperbolic Polariton Propagation with Negative Phase Velocity. *Nat. Photonics* **2015**, *9*, 674–678.

(110) Pavlidis, G.; Schwartz, J. J.; Matson, J. R.; Folland, T. G.; Liu, S.; Edgar, J. H.; Caldwell, J. D.; Centrone, A. Experimental Confirmation of Long Hyperbolic Polariton Lifetimes in Monoisotopic (10B) Hexagonal Boron Nitride at Room Temperature. *APL Mater.* **2021**, *9* (9), DOI: 10.1063/5.0061941.

(111) Ambrosio, A.; Jauregui, L. A.; Dai, S.; Chaudhary, K.; Tamagnone, M.; Fogler, M. M.; Basov, D. N.; Capasso, F.; Kim, P.; Wilson, W. L. Mechanical Detection and Imaging of Hyperbolic Phonon Polaritons in Hexagonal Boron Nitride. *ACS Nano* **2017**, *11* (9), 8741–8746.

(112) Kim, K.-H.; No, Y.-S.; Chang, S.; Choi, J.-H.; Park, H.-G. Invisible Hyperbolic Metamaterial Nanotube at Visible Frequency. *Sci. Rep.* **2015**, *5* (1), 16027. https://doi.org/10.1038/srep16027.

(113) Cassabois, G.; Valvin, P.; Gil, B. Hexagonal Boron Nitride Is an Indirect Bandgap Semiconductor. *Nat. Photonics* **2016**, *10*, 262–266.

(114) Watanabe, K.; Taniguchi, T.; Kanda, H. Direct-Bandgap Properties and Evidence for Ultraviolet Lasing of Hexagonal Boron Nitride Single Crystal. *Nat. Mater.* **2004**, *3*, 404–409.

(115) Dunkelberger, A. D.; Ellis, C. T.; Ratchford, D. C.; Giles, A. J.; Kim, M.; Kim, C. S.; Spann, B. T.; Vurgaftman, I.; Tischler, J. G.; Long, J. P.; Glembocki, O. J.; Owrutsky, J. C.; Caldwell, J. D. Active Tuning of Surface Phonon Polariton Resonances via Carrier Photoinjection. *Nat. Photonics* **2018**, *12* (1), 50–56. https://doi.org/10.1038/s41566-017-0069-0.

(116) Spann, B. T.; Compton, R.; Ratchford, D.; Long, J. P.; Dunkelberger, A. D.; Klein, P. B.; Giles, A. J.; Caldwell, J. D.; Owrutsky, J. C. Photoinduced Tunability of the Reststrahlen Band in 4H-SiC. *Phys.*

Rev. B **2016**, *93* (8), 085205. https://doi.org/10.1103/PhysRevB.93.085205.

(117) Dunkelberger, A. D.; Ratchford, D. C.; Grafton, A. B.; Breslin, V. M.; Ryland, E. S.; Katzer, D. S.; Fears, K. P.; Weiblen, R. J.; Vurgaftman, I.; Giles, A. J.; Ellis, C. T.; Tischler, J. G.; Caldwell, J. D.; Owrutsky, J. C. Ultrafast Active Tuning of the Berreman Mode. *ACS Photonics* **2020**, *7* (1), 279–287. https://doi.org/10.1021/acsphotonics.9b01578.

(118) Folland, T. G.; Fali, A.; White, S. T.; Matson, J. R.; Liu, S.; Aghamiri, N. A.; Edgar, J. H.; Haglund, R. F.; Abate, Y.; Caldwell, J. D. Reconfigurable Infrared Hyperbolic Metasurfaces Using Phase Change Materials. *Nat. Commun.* **2018**, *9*, 4371. https://doi.org/10.1038/s41467-018-06858-y.

(119) Fali, A.; White, S. T.; Folland, T. G.; He, M.; Aghamiri, N. A.; Liu, S.; Edgar, J. H.; Caldwell, J. D.; Haglund, R. F.; Abate, Y. Refractive Index-Based Control of Hyperbolic Phonon-Polariton Propagation. *Nano Lett.* **2019**, *19* (11), 7725–7734. https://doi.org/10.1021/acs.nanolett.9b02651.

(120) Sternbach, A. J.; Chae, S. H.; Latini, S.; Rikhter, A. A.; Shao, Y.; Li, B.; Rhodes, D.; Kim, B.; Schuck, P. J.; Xu, X.; Zhu, X.-Y.; Averitt, R. D.; Hone, J.; Fogler, M. M.; Rubio, A.; Basov, D. N. Programmable Hyperbolic Polaritons in van Der Waals Semiconductors. *Science (80-.).* **2021**, *371* (6529), 617–620.

(121) Chaudhary, K.; Tamagnone, M.; Yin, X.; Spägele, C. M.; Oscurato, S. L.; Li, J.; Persch, C.; Li, R.; Rubin, N. A.; Jauregui, L. A.; Watanabe, K.; Taniguchi, T.; Kim, P.; Wuttig, M.; Edgar, J. H.; Ambrosio, A.; Capasso, F. Polariton Nanophotonics Using Phase-Change Materials. *Nat. Commun.* **2019**, *10* (1), 4487. https://doi.org/10.1038/s41467-019-12439-4.

(122) Yoo, D.; de León-Pérez, F.; Pelton, M.; Lee, I.-H.; Mohr, D. A.; Raschke, M. B.; Caldwell, J. D.; Martín-Moreno, L.; Oh, S.-H. Ultrastrong Plasmon-Phonon Coupling via Epsilon-near-Zero Nanocavities. *Nat. Photonics* **2021**, *15*, 125–130.

(123) Gubbin, C. R.; Berte, R.; Meeker, M. A.; Giles, A. J.; Ellis, C. T.; Tischler, J. G.; Wheeler, V. D.; Maier, S. A.; Caldwell, J. D.; De Liberato, S. Hybrid Longitudinal-Transverse Phonon Polaritons. *Nat. Commun.* **2019**, *10*, 1682. https://doi.org/10.1038/s41467-019-09414-4.

(124) Runnerstrom, E. L.; Kelley, K. P.; Folland, T. G.; Nolen, J. R.; Engheta, N.; Caldwell, J. D.; Maria, J. P. Polaritonic Hybrid-Epsilon-near-Zero Modes: Beating the Plasmonic Confinement vs Propagation-Length Trade-Off with Doped Cadmium Oxide Bilayers. *Nano Lett.* **2019**, *19* (2), 948–957.

https://doi.org/10.1021/acs.nanolett.8b04182.

(125) Autore, M.; Li, P.; Dolado, I.; Alfaro-Mozaz, F. J.; Esteban, R.; Atxabal, A.; Casanova, F.; Hueso, L. E.; Alonso-Gonzalez, P.; Aizpurua, J.; Nikitin, A. Y.; Velez, S.; Hillenbrand, R. Boron Nitride Nanoresonators for Phonon-Enhanced Molecular Vibrational Spectroscopy at the Strong Coupling Limit. *Light Sci. Appl.* **2018**, *7*, 17172. https://doi.org/doi.org:10.1038/lsa.2017.172.

(126) Autore, M.; Li, P.; Dolado, I.; Alfaro-Mozaz, F. J.; Esteban, R.; Atxabal, A.; Casanova, F.; Hueso, L. E.; Alonso-González, P.; Aizpurua, J.; Nikitin, A. Y.; Vélez, S.; Hillenbrand, R. Boron Nitride Nanoresonators for Phonon-Enhanced Molecular Vibrational Spectroscopy at the Strong Coupling Limit. *Light Sci. Appl.* **2018**, *7* (4), 17172–17172. https://doi.org/10.1038/lsa.2017.172.

(127) Adato, R.; Yanik, A. A.; Amsden, J. J.; Kaplan, D. L.; Omenetto, F. G.; Hong, M. K.; Erramilli, S.; Altug, H. Ultra-Sensitive Vibrational Spectroscopy of Protein Monolayers with Plasmonic Nanoantenna Arrays. *Proc. Natl. Acad. Sci. USA* **2009**, *106* (46), 19227–19232.

(128) Rodrigo, D.; Limaj, O.; Janner, D.; Etezadi, D.; Garcia de Abajo, F. J.; Pruneri, V.; Altug, H. Mid-Infrared Plasmonic Biosensing with Graphene. *Science (80-.).* **2015**, *349* (6244), 165–168.

(129) Neubrech, F.; Huck, C.; Weber, K.; Pucci, A.; Giessen, H. Surface-Enhanced Infrared Spectroscopy Using Resonant Nanoantennas. *Chem. Rev.* **2017**, *117* (7), 5110–5145. https://doi.org/10.1021/acs.chemrev.6b00743.

(130) Yu, N.; Genevet, P.; Kats, M. A.; Aieta, F.; Tetienne, J.-P.; Capasso, F.; Gaburro, Z. Light Propagation with Phase Discontinuities: Generalized Laws of Reflection and Refraction. *Science (80-.).* **2011**, *334* (6054), 333–337.

(131) Martin-Sanchez, J.; Duan, J.; Taboada-Gutiérrez, J.; Alvarez-Perez, G.; Voronin, K. V.; Prieto, I.; Ma, W.; Bao, Q.; Volkov, V. S.; Hillenbrand, R.; Nikitin, A.; Alonso-González, P. Focusing of In-Plane Hyperbolic Polaritons in van Der Waals Crystals with Tailored Infrared Nanoantennas. Science advances. **2021**, 7.41: eabj0127.

(132) Zheng, Z.; Jiang, J.; Xu, N.; Wang, X.; Huang, W.; Ke, Y.; Chen, H.; Deng, S. Controlling and Focusing of In-Plane Hyperbolic Phonon Polaritons in Alpha-MoO3 with Plasmonic Antenna. Adv. Mater. **2021**, 2104164. https://doi.org/10.1002/adma.202104164.

(133) Duan, J.; Álvarez-Pérez, G.; Tresguerres-Mata, A. I. F.; Taboada-Gutiérrez, J.; Voronin, K. V.;

Bylinkin, A.; Chang, B.; Xiao, S.; Liu, S.; Edgar, J. H.; Martín, J. I.; Volkov, V. S.; Hillenbrand, R.; Martín-Sánchez, J.; Nikitin, A. Y.; Alonso-González, P. Planar Refraction and Lensing of Highly Confined Polaritons in Anisotropic Media. *Nat. Commun.* **2021**, *12* (1), 4325. https://doi.org/10.1038/S41467-021-24599-3.

(134) He, M.; Halimi, S. I.; Folland, T. G.; Sunku, S.; Liu, S.; Edgar, J. H.; Basov, D. N.; Weiss, S. M.; Caldwell, J. D. Guided Mid-IR and Near-IR Light within a Hybrid Hyperbolic-Material/Silicon Waveguide Heterostructure. *Adv. Mater.* **2021**, *33* (11), 2004305. https://doi.org/10.1002/adma.202004305.

(135) Ramezani, M.; Berghuis, M.; Gómez Rivas, J. Strong Light–Matter Coupling and Exciton-Polariton Condensation in Lattices of Plasmonic Nanoparticles [Invited]. *J. Opt. Soc. Am. B* **2019**, *36* (7), E88–E103. https://doi.org/10.1364/JOSAB.36.000E88.

(136) Woessner, A.; Lundeberg, M. B.; Gao, Y.; Principi, A.; Alonso-Gonzalez, P.; Carrega, M.; Watanabe, K.; Taniguchi, T.; Vignale, G.; Polini, M.; Hone, J.; Hillenbrand, R.; Koppens, F. H. L.; Taniguchi, K.; Vignale, G.; Polini, M.; Hone, J.; Hillenbrand, R.; Koppens, F. H. L. Highly Confined Low-Loss Plasmons in Graphene-Boron Nitride Heterostructures. *Nat. Mater.* **2015**, *14*, 421–425.

(137) Brar, V. W.; Jang, M. S.; Sherrott, M.; Kim, S.; Lopez, J. J.; Kim, L. B.; Choi, M.; Atwater, H. A. Hybrid Surface-Phonon-Plasmon Polariton Modes in Graphene/Monolayer h-BN Heterostructures. *Nano Lett.* **2014**, *14* (7), 3876–3880.

(138) Brar, V. W.; Jang, M. S.; Sherrott, M.; Lopez, J. J.; Atwater, H. A. Highly Confined Tunable Mid-Infrared Plasmonics in Graphene Nanoresonators. *Nano Lett.* **2013**, *13*, 2541–2547.

(139) Kumar, A.; Low, T.; Fung, K. H.; Avouris, P.; Fang, N. X. Tunable Light-Matter Interaction and the Role of Hyperbolicity in Graphene-HBN System. *Nano Lett.* **2015**, *15* (5), 3172–3180.

(140) Cao, Y.; Fatemi, V.; Fang, S.; Watanabe, K.; Taniguchi, T.; Kaxiras, E.; Jarillo-Herrero, P. Unconventional Superconductivity in Magic-Angle Graphene Superlattices. *Nature* **2018**, *556*, 43–50.

(141) L., S. A.; J., F. E.; W., B. A.; Joe, F.; Kenji, W.; Takashi, T.; A., K. M.; David, G.-G. Emergent Ferromagnetism near Three-Quarters Filling in Twisted Bilayer Graphene. *Science (80-.).* **2019**, *365* (6453), 605–608. https://doi.org/10.1126/science.aaw3780.

(142) Hu, G.; Ou, Q.; Si, G.; Wu, Y.; Wu, J.; Dai, Z.; Krasnok, A.; Mazor, Y.; Zhang, Q.; Bao, Q.; Qiu, C. W.; Alù, A. Topological Polaritons and Photonic Magic Angles in Twisted α-MoO3 Bilayers. *Nature* **2020**. https://doi.org/10.1038/s41586-020-2359-9.

(143) Chen, M.; Lin, X.; Dinh, T. H.; Zheng, Z.; Shen, J.; Ma, Q.; Chen, H.; Jarillo-Herrero, P.; Dai, S. Configurable Phonon Polaritons in Twisted α-MoO3. *Nat. Mater.* **2020**. https://doi.org/10.1038/s41563-020-0732-6.

(144) Hu, G.; Krasnok, A.; Mazor, Y.; Qiu, C.-W.; Alù, A. Moiré Hyperbolic Metasurfaces. *Nano Lett.* **2020**, *20* (5), 3217–3224. https://doi.org/10.1021/acs.nanolett.9b05319.

(145) Correas-Serrano, D.; Alù, A.; Gomez-Diaz, J. S. Plasmon Canalization and Tunneling over Anisotropic Metasurfaces. *Phys. Rev. B* **2017**, *96* (7), 75436. https://doi.org/10.1103/PhysRevB.96.075436.

(146) Zhang, Q.; Ou, Q.; Hu, G.; Liu, J.; Dai, Z.; Fuhrer, M. S.; Bao, Q.; Qiu, C.-W. Hybridized Hyperbolic Surface Phonon Polaritons at Alpha-MoO3 and Polar Dielectric Interfaces. *Nano Lett.* **2021**, *21* (7), 3112–3119.

(147) Duan, J.; Alvarez-Perez, G.; Voronin, K. V.; Prieto, I.; Taboada-Gutiérrez, J.; Volkov, V. S.; Martin-Sanchez, J.; Nikitin, A. Y.; Alonso-González, P. Enabling Propagation of Anisotropic Polaritons along Forbidden Directions via a Topological Transition. *Sci. Adv.* **2021**, *7* (14), eabf2690.

(148) Bylinkin, A.; Schnell, M.; Autore, M.; Calavalle, F.; Li, P.; Taboada-Gutiérrez, J.; Liu, S.; H., E. J.; Casanova, F.; Hueso, L. E.; Alonso-González, P.; Nikitin, A. Y.; Hillenbrand, R. Real-Space Observation of Vibrational Strong Coupling between Propagating Phonon Polaritons and Organic Molecules. *Nat. Photonics* **2021**, *15*, 197–202.

(149) Galfsky, T.; Krishnamoorthy, H. N. S.; Newman, W.; Narimanov, E. E.; Jacob, Z.; Menon, V. M. Active Hyperbolic Metamaterials: Enhanced Spontaneous Emission and Light Extraction. *Optica* **2015**, *2* (1), 62–65. https://doi.org/10.1364/OPTICA.2.000062.

(150) Wu, X.; Fu, C.; Zhang, Z. M. Near-Field Radiative Heat Transfer between Two α-MoO3biaxial Crystals. *J. Heat Transfer* **2020**, *142* (7), 072802. https://doi.org/10.1115/1.4046968.

(151) Salihoglu, H.; Iyer, V.; Taniguchi, T.; Watanabe, K.; Ye, P. D.; Xu, X. Energy Transport by Radiation in Hyperbolic Material Comparable to Conduction. *Adv. Funct. Mater.* **2020**, *30* (6), 1905830.

https://doi.org/10.1002/adfm.201905830.

(152) Chen, D.-Z. A.; Narayanaswamy, A.; Chen, G. Surface Phonon-Polariton Mediated Thermal Conductivity Enhancement of Amorphous Thin Films. *Phys. Rev. B* **2005**, *72*, 155435.

(153) Wu, Y.; Ordonez-Miranda, J.; Gluchko, S.; Anufriev, R.; De Sousa Meneses, D.; Del Campo, L.; Volz, S.; Nomura, M. Enhanced Thermal Conduction by Surface Phonon-Polaritons. *Sci. Adv.* **2020**, *6* (40), eabb4461.

(154) Sood, A. K.; Menendez, J.; Cardona, M.; Ploog, K. Resonance Raman Scattering by Confined LO and TO Phonons in GaAs-AlAs Superlattices. *Phys. Rev. Lett.* **1985**, *54*, 2111.

(155) Fasol, G.; Tanaka, M.; Sakaki, H.; Horikoshi, Y. Interface Roughness and the Dispersion of Confined LO Phonons in GaAs/AlAs Quantum Wells. *Phys. Rev. B* **1988**, *38* (9), 6056–6065.

(156) Wang, Z. P.; Jiang, D. S.; Ploog, K. Raman Scattering of (GaAs)n(AlAs)n Superlattices. *Solid State Commun.* **1988**, *65* (7), 661–663. https://doi.org/https://doi.org/10.1016/0038-1098(88)90359-6.

(157) Mowbray, D. J.; Cardona, M.; Ploog, K. Confined LO Phonons in GaAs/AlAs Superlattices. *Phys. Rev. B* **1991**, *43* (2), 1598–1603.

(158) Nakayama, M.; Ishida, M.; Sano, N. Interface-Phonon Polaritons in GaAs/AlAs Heterostructures. *Surf. Sci.* **1990**, *228* (1), 131–134. https://doi.org/https://doi.org/10.1016/0039-6028(90)90274-C.

(159) Huber, A.; Egeler, T.; Ettmüller, W.; Rothfritz, H.; Tränkle, G.; Abstreiter, G. Interface Phonons in GaAs/AlAs Superlattices Studied by Micro-Raman Spectroscopy. *Superlattices Microstruct.* **1991**, *9* (3), 309–311. https://doi.org/https://doi.org/10.1016/0749-6036(91)90248-P.

(160) López, C.; Springett, R. J.; Nicholas, R. J.; Walker, P. J.; Mason, N. J.; Hayes, W. Interface Studies of InAs/GaSb Superlattices by Raman Scattering. *Surf. Sci.* **1992**, *267* (1), 176–180. https://doi.org/https://doi.org/10.1016/0039-6028(92)91115-R.

(161) Berte, R.; Gubbin, C. R.; Wheeler, V. D.; Giles, A. J.; Giannini, V.; Maier, S. A.; De Liberato, S.; Caldwell, J. D. Sub-Nanometer Thin Oxide Film Sensing with Localized Surface Phonon Polaritons. *ACS Photonics* **2018**, *5* (7), 2807–2815. https://doi.org/10.1021/acsphotonics.7b01482.

(162) Gubbin, C. R.; De Liberato, S. Nonlocal Scattering Matrix Description of Anisotropic Polar Heterostructures. *Phys. Rev. B* **2020**, *102*, 235301.

(163) Gubbin, C. R.; De Liberato, S. Impact of Phonon Nonlocality on Nanogap and Nanolayer Polar Resonators. *Phys. Rev. B* **2020**, *102*, 201302(R).

(164) Vuong, T. Q. P.; Liu, S.; Van der Lee, A.; Cusco, R.; Artus, L.; Michel, T.; Valvin, P.; Edgar, J. H.; Cassabois, G.; Gil, B. Isotope Engineering of van Der Waals Interactions in Hexagonal Boron Nitride. *Nat. Mater.* **2018**, *17*, 152–158.

(165) Lane, M. Midinfrared Optical Constants of Calcite and Their Relationship to Particle Size Effects in Thermal Emission Spectra of Granular Calcite. *J. Geophys. Res.* **1999**, *104*, 14099–14108. https://doi.org/10.1029/1999JE900025.

(166) Zhao, K.; Huang, F.; Dai, C.-M.; Li, W.; Chen, S.-Y.; Jiang, K.; Huang, Y.-P.; Hu, Z.; Chu, J. Temperature Dependence of Phonon Modes, Optical Constants, and Optical Band Gap in Two-Dimensional ReS2 Films. *J. Phys. Chem. C* **2018**, *122* (51), 29464–29469.

(167) Garcia de Abajo, F. J. Optical Excitations in Electron Microscopy. *Rev. Mod. Phys.* **82AD**, No. 209.

(168) Aizpura, J.; Rivacoba, A. Nonlocal Effects in the Plasmons of Nanowires and Nanocavities Excited by Fast Electron Beams. *Phys. Rev. B* **2008**, *78*, 035404.

(169) Abd El-Fattah, Z. M.; Mikhitaryan, V.; Brede, J.; Fernandez, L.; Li, C.; Guo, Q.; Ghosh, A.; Echarri, A. R.; Naveh, D.; Xia, F.; Ortega, J. E.; Garcia de Abajo, F. J. Plasmonics in Atomically Thin Crystalline Silver Films. *ACS Nano* **2019**, *13* (7), 7771–7779.

(170) Echarri, A. R.; Cox, J. D.; Garcia de Abajo, F. J. Quantum Effects in the Acoustic Plasmons of Atomically Thin Heterostructures. *Optica* **2019**, *6* (5), 630–641.

(171) Lee, I.-H.; Martin-Moreno, L.; Mohr, D. A.; Khaliji, K.; Low, T.; Oh, S.-H. Anisotropic Acoustic Plasmons in Black Phosphorus. ACS photonics. **2018**. 5.6 : 2208-2216.

(172) Iranzo, D. A.; Nanot, S.; Dias, E. J. C.; Epstein, I.; Peng, C.; Efetov, D. K.; Lundeberg, M. B.; Parret, R.; Osmond, J.; Hong, J. Y.; Kong, J.; Englund, D. R.; Peres, N. M. R.; Koppens, F. H. L. Probing the Ultimate Plasmon Confinement Limits with a van Der Waals Heterostructure. *Science (80-.).* **2018**, *360* (6386), 291–295. https://doi.org/10.1126/SCIENCE.AAR8438.

(173) Scholl, J. A.; Garcia-Etxarri, A.; Koh, A. L.; Dionne, J. A. Observation of Quantum Tunneling between Two Plasmonic Nanoparticles. *Nano Lett.* **2013**, *13*, 564–569.

(174) Rossouw, D.; Couillard, M.; Vickery, J.; Kumacheva, E.; Botton, G. A. Multipolar Plasmonic

Resonances in Silver Nanowire Antennas Imaged with a Subnanometer Electron Probe. *Nano Lett.* **2011**, *11* (4), 1499–1504. https://doi.org/10.1021/nl200634w.

(175) Rajabali, S.; Cortese, E.; Beck, M.; De Liberato, S.; Faist, J.; Scalari, G. Polaritonic Nonlocality in Light–Matter Interaction. *Nat. Photonics* **2021**, *15* (9), 690–695. https://doi.org/10.1038/s41566-021-00854-3.

(176) Ciraci, C.; Hill, R. T.; Mock, J. J.; Urzhumov, Y.; Fenandez-Dominguez, A. I.; Maier, S. A.; Pendry, J. B.; Chilkoti, A.; Smith, D. R. Probing the Ultimate Limits of Plasmonic Enhancement. *Sci.* **2012**, *337*, 1072–1074.

(177) Ciracì, C.; Pendry, J. B.; Smith, D. R. Hydrodynamic Model for Plasmonics: A Macroscopic Approach to a Microscopic Problem. *ChemPhysChem* **2013**, *14* (6), 1109–1116. https://doi.org/https://doi.org/10.1002/cphc.201200992.

(178) Mortensen, N. A.; Raza, S.; Wubs, M.; Søndergaard, T.; Bozhevolnyi, S. I. A Generalized Non-Local Optical Response Theory for Plasmonic Nanostructures. *Nat. Commun.* **2014**, *5* (1), 3809. https://doi.org/10.1038/ncomms4809.

(179) Gubbin, C. R.; De Liberato, S. Quantum Theory of Longitudinal-Transverse Polaritons in Nonlocal Thin Films. Physical Review Applied. **2022**. 17.1: 014037.

(180) Caldwell, J. D.; Glembocki, O. J.; Francescato, Y.; Sharac, N.; Giannini, V.; Bezares, F. J.; Long, J. P.; Owrutsky, J. C.; Vurgaftman, I.; Tischler, J. G.; Wheeler, V. D.; Bassim, N. D.; Shirey, L. M.; Kasica, R.; Maier, S. A. Low-Loss, Extreme Subdiffraction Photon Confinement via Silicon Carbide Localized Surface Phonon Polariton Resonators. *Nano Lett.* **2013**, *13* (8), 3690–3697. https://doi.org/10.1021/nl401590g.

(181) Ellis, C. T.; Tischler, J. G.; Glembocki, O. J.; Bezares, F. J.; Giles, A. J.; Kasica, R.; Shirey, L.; Owrutsky, J. C.; Chigrin, D. N.; Caldwell, J. D. Aspect-Ratio Driven Evolution of High-Order Resonant Modes and near-Field Distributions in Localized Surface Phonon Polariton Nanostructures. *Sci. Rep.* **2016**, *6* (1), 1–11. https://doi.org/10.1038/srep32959.

(182) Nakashima, S.; Harima, H. Raman Investigation of SiC Polytypes. *Phys. Status Solidi A Appl. Res.* **1997**, *162*, 39.

(183) Sunku, S. S.; Ni., G. X.; Jiang, B. Y.; Yoo, H.; Sternbach, A.; McLeod, A. S.; Stauber, T.; Xiong, L.;

Taniguchi, T.; Watanabe, K.; Kim, P.; Fogler, M. M.; Basov, D. N. Photonic Crystals for Nano-Light in Moire Graphene Superlattices. *Science (80-.).* **2018**, *362* (6419), 1153–1156.

(184) Hesp, N. C. H.; Torre, I.; Rodan-Legrain, D.; Novelli, P.; Cao, Y.; Carr, S.; Fang, S.; Stepanov, P.; Barcons-Ruiz, D.; Herzig Sheinfux, H.; Watanabe, K.; Taniguchi, T.; Efetov, D. K.; Kaxiras, E.; Jarillo-Herrero, P.; Polini, M.; Koppens, F. H. L. Observation of Interband Collective Excitations in Twisted Bilayer Graphene. *Nat. Phys.* **2021**. https://doi.org/10.1038/s41567-021-01327-8.

(185) Ni, G. X.; Wang, H.; Wu, J. S.; Fei, Z.; Goldflam, M. D.; Keilmann, F.; Özyilmaz, B.; Castro Neto, A. H.; Xie, X. M.; Fogler, M. M.; Basov, D. N. Plasmons in Graphene Moiré Superlattices. *Nat. Mater.* **2015**, *14* (12), 1217–1222. https://doi.org/10.1038/nmat4425.

(186) Lin, X.; Liu, Z.; Stauber, T.; Gómez-Santos, G.; Gao, F.; Chen, H.; Zhang, B.; Low, T. Chiral Plasmons with Twisted Atomic Bilayers. *Phys. Rev. Lett.* **2020**, *125* (7), 77401. https://doi.org/10.1103/PhysRevLett.125.077401.

(187) Zhang, L.; Wu, F.; Hou, S.; Zhang, Z.; Chou, Y.-H.; Watanabe, K.; Taniguchi, T.; Forrest, S. R.; Deng, H. Van Der Waals Heterostructure Polaritons with Moire-Induced Nonlinearity. *Nature* **2021**, *591*, 61–65.

(188) Gubbin, C. R.; De Liberato, S.; Folland, T. G. Surface phonon polaritons for infrared optoelectronics. *Journal of Applied Physics **2022**. 131.3: 030901.*

(189) Ohtani, K.; Meng, B.; Franckié, M.; Bosco, L.; Ndebeka-Bandou, C.; Beck, M.; Faist, J. An Electrically Pumped Phonon-Polariton Laser. *Sci. Adv.* **2021**, *5* (7), eaau1632. https://doi.org/10.1126/sciadv.aau1632.